

Musculoskeletal model-based inverse dynamic analysis under ambulatory conditions using inertial motion capture

Karatsidis, Angelos; Jung, Moonki; Schepers, Martin; Bellusci, Giovanni; de Zee, Mark; Veltink, Peter H.; Andersen, Michael Skipper

Published in:
Medical Engineering & Physics

DOI (link to publication from Publisher):
[10.1016/j.medengphy.2018.12.021](https://doi.org/10.1016/j.medengphy.2018.12.021)

Creative Commons License
CC BY-NC-ND 4.0

Publication date:
2019

Document Version
Accepted author manuscript, peer reviewed version

[Link to publication from Aalborg University](#)

Citation for published version (APA):
Karatsidis, A., Jung, M., Schepers, M., Bellusci, G., de Zee, M., Veltink, P. H., & Andersen, M. S. (2019). Musculoskeletal model-based inverse dynamic analysis under ambulatory conditions using inertial motion capture. *Medical Engineering & Physics*, 65, 68-77. <https://doi.org/10.1016/j.medengphy.2018.12.021>

General rights

Copyright and moral rights for the publications made accessible in the public portal are retained by the authors and/or other copyright owners and it is a condition of accessing publications that users recognise and abide by the legal requirements associated with these rights.

- Users may download and print one copy of any publication from the public portal for the purpose of private study or research.
- You may not further distribute the material or use it for any profit-making activity or commercial gain
- You may freely distribute the URL identifying the publication in the public portal -

Take down policy

If you believe that this document breaches copyright please contact us at vbn@aub.aau.dk providing details, and we will remove access to the work immediately and investigate your claim.

Title:

Musculoskeletal model-based inverse dynamic analysis under ambulatory conditions using inertial motion capture

Authors:

Angelos Karatsidis^{1,2}, Moonki Jung³, H. Martin Schepers¹, Giovanni Bellusci⁴, Mark de Zee⁴, Peter H. Veltink², Michael Skipper Andersen⁵

Affiliations:

¹Xsens Technologies B.V., Enschede 7521 PR, The Netherlands

²Department of Biomedical Signals and Systems, Faculty of Electrical Engineering, Mathematics and Computer Science, University of Twente, Enschede 7500 AE, The Netherlands

³AnyBody Technology A/S, Aalborg 9220, Denmark

⁴Department of Health Science and Technology, Aalborg University, Aalborg 9220, Denmark

⁵Department of Materials and Production, Aalborg University, Aalborg 9220, Denmark

Corresponding author:

Angelos Karatsidis, Address: Xsens Technologies B.V., Pantheon 6-8, Enschede 7521 PR, The Netherlands, E-mail: angelos.karatsidis@xsens.com, Tel.: +31 88 97367 36, Fax: +31 88 97367 01

Keywords:

musculoskeletal modeling, inertial motion capture, inverse dynamics, ground reaction forces and moments, gait analysis

Wordcount:

Abstract: 197 words

Main text: 3582 words

Abstract

Inverse dynamic analysis using musculoskeletal modeling is a powerful tool, which is utilized in a range of applications to estimate forces in ligaments, muscles, and joints, non-invasively. To date, the conventional input used in this analysis is derived from optical motion capture (OMC) and force plate (FP) systems, which restrict the application of musculoskeletal models to gait laboratories. To address this problem, we propose the use of inertial motion capture to perform musculoskeletal model-based inverse dynamics by utilizing a universally applicable ground reaction force and moment (GRF&M) prediction method. Validation against a conventional laboratory-based method showed excellent Pearson correlations for sagittal plane joint angles of ankle, knee, and hip ($\rho = 0.95, 0.99, \text{ and } 0.99$, respectively) and root-mean-squared-differences (RMSD) of $4.1 \pm 1.3^\circ$, $4.4 \pm 2.0^\circ$, and $5.7 \pm 2.1^\circ$, respectively. The GRF&M predicted using IMC input were found to have excellent correlations for three components (vertical: $\rho = 0.97$, RMSD= 9.3 ± 3.0 %BW, anteroposterior: $\rho = 0.91$, RMSD= 5.5 ± 1.2 %BW, sagittal: $\rho = 0.91$, RMSD= 1.6 ± 0.6 %BW*BH), and strong correlations for mediolateral ($\rho = 0.80$, RMSD= 2.1 ± 0.6 %BW) and transverse ($\rho = 0.82$, RMSD= 0.2 ± 0.1 %BW*BH). The proposed IMC-based method removes the complexity and space-restrictions of OMC and FP systems and could enable applications of musculoskeletal models in either monitoring patients during their daily lives or in wider clinical practice.

1. Introduction

Assessment of muscle, joint, and ligament forces is important to understand the mechanical and physiological mechanisms of human movement. To date, the measurement of such in-vivo forces is a challenging task. For this reason, computer-based musculoskeletal models have been widely used to estimate the variables of interest non-invasively [1, 2].

The most common approach used in musculoskeletal modeling is the method of the inverse dynamics [3]. This analysis utilizes the equations of motion with input from human body kinematics in conjunction with kinetics obtained from external forces [4], to estimate joint reaction and muscle forces, as well as net joint moments using muscle recruitment methods [5]. Measurements of the external forces are typically required and measured using force plates (FPs), however, the use of FPs has several limitations. First, subjects tend to alter their natural gait patterns in order to hit the small and fixed measurement area of a plate [6]. In addition, this static and limited measurement area, impedes the assessment of several consecutive steps, when only a couple of FPs are available. Finally, the combined use of FP with motion input introduces a dynamic inconsistency, which results to residual forces and moments in the inverse dynamics. [7, 8].

Several studies have proposed replacing the FP input with wearable devices such as shoes with three-dimensional force and torque sensors beneath the sole [9, 10, 11]. In a similar fashion, pressure insoles were proposed to reconstruct the complete ground reaction forces and moments (GRF&M) from pressure distributions [12, 13, 14]. Although these wearable devices are suitable for the assessment of external forces, the increased height and weight of the shoes equipped with force/torque sensors [15, 16], as well as the repeatability of the pressure sensors [17] are considered important limitations.

Recent research has suggested the replacement of the force input with predictions derived solely from motion input [18, 19, 20, 21, 22, 23]. In these studies, human body kinematics are combined with the inertial properties of the body

52 segments, from which Newton-Euler equations are utilized to compute the exter-
 53 nal forces and moments. Since the system of equations becomes indeterminate
 54 during the double stance of gait, each of the aforementioned studies focused on
 55 methods to solve this issue. Ren *et al.* [19] suggested a gait event-based func-
 56 tion which is only applicable in gait, while Oh *et al.* [20] and Choi *et al.* [21]
 57 suggested methods based on a machine learning that require a training database
 58 and thus are not applicable for movements not included in that database. A
 59 last approach enables the universal application of these methods using a muscle
 60 recruitment approach has shown promising performance for various activities of
 61 daily living [22] and sports [23].

62 The majority of the existing research which studied the prediction of GRF&M,
 63 used conventional optical motion capture (OMC) input. Despite the high ac-
 64 curacy of this method in tracking marker trajectories, its dependence on lab-
 65 oratory equipment restricts possible applications during daily life activities or
 66 in wider clinical practice. In the previous decade, ambulatory motion tracking
 67 systems based on inertial measurement units (IMUs), have been proposed as a
 68 suitable alternative for estimating 3D segment kinematics [24, 25, 26, 27]. A
 69 key benefit of such systems is that they can be applied in virtually any environ-
 70 ment without depending on external infrastructure, such as cameras. Driven
 71 by these advances in inertial motion capture (IMC), recent work of the authors
 72 demonstrated its ability to estimate three-dimensional GRF&M [28], which were
 73 distributed between the feet using a smooth transition assumption concept [19].
 74 However, limitations of that approach is that it is only valid for gait and has no
 75 muscle, bone or ligament force estimate capabilities.

76 To date, the use of detailed musculoskeletal modeling with kinematic inputs
 77 from IMUs has only received limited attention. Koning *et al.* [29] previously
 78 demonstrated the feasibility of kinematically driving a musculoskeletal model
 79 using only orientations from IMUs. However, that study only compared the
 80 kinematics of the musculoskeletal model, without any inverse dynamic calcula-
 81 tions.

82 The aim of this study was to develop a workflow to perform musculoskeletal

83 model-based inverse dynamics using exclusively IMC input, applicable in am-
84 bulatory environments and validate it against a conventional laboratory-based
85 approach.

86 **2. Methods**

87 *2.1. Subjects*

88 The experimental data was collected at the Human Performance Labora-
89 tory, at the Department of Health Science and Technology, Aalborg University,
90 Aalborg, Denmark following the ethical guidelines of The Scientific Ethical Com-
91 mittee for the Region of North Jutland (Den Videnskabsetiske Komit for Region
92 Nordjylland). Eleven healthy male individuals with no present musculoskeletal
93 or neuromuscular disorders volunteered for the study (age: 31.0 ± 7.2 years;
94 height: 1.81 ± 0.06 m; weight: 77.3 ± 9.2 kg; body mass index (BMI): $23.6 \pm$
95 2.4 kg/m²). All participants provided written informed consent, prior to data
96 collection.

97 *2.2. Instrumentation*

98 Full-body IMC data were collected using the Xsens MVN Link (Xsens Tech-
99 nologies B.V., Enschede, the Netherlands), in which 17 IMUs were mounted on
100 the head, sternum, pelvis, upper legs, lower legs, feet, shoulders, upper arms,
101 forearms and hands using the dedicated clothing. The exact location of each
102 sensor on the respective segment followed the manufacturer guidelines described
103 in the manual of Xsens MVN [30]. The affiliated software Xsens MVN Studio
104 4.2.4 was used to track the IMU orientations with respect to an earth-based
105 coordinate frame [24, 25]. Segment orientations were obtained by applying the
106 IMU-to-segment alignment, found using a known upright pose (N-pose) per-
107 formed by the subject at a known moment in time, while taking specific care
108 to minimize the effect of magnetic disturbances. In addition, this information
109 is fused with updates regarding the joints and external contacts to limit the
110 position drift [26].

For validation purposes, an OMC system utilizing 8 infrared high speed cameras (Oqus 300 series, Qualisys AB, Gothenburg, Sweden) and the software Qualisys Track Manager 2.12 (QTM) were used to track the trajectories of 53 reflective markers mounted on the human body, as described in the Appendix of [28]. In addition, three FP systems (AMTI OR6-7-1000, Advanced Mechanical Technology, Inc., Watertown, MA, USA) embedded in the floor of the laboratory, were utilized using QTM to record the GRF&Ms. Both IMC and OMC systems sampled data at a frequency of 240 Hz, while the FP system sampled data at 2400 Hz and subsequently downsampled to 240 Hz to match the IMC and OMC sampling rate.. A second-order forward-backward low-pass Butterworth filter was applied to the reflective marker trajectories and measured GRF&M, with cut-off frequencies of 6 Hz and 15 Hz, respectively.

2.3. Experimental protocol

For each participant, the body dimensions were extracted using a conventional tape following the guidelines of Xsens. During the data collection, the subjects were instructed to walk barefoot in three different walking speeds (comfortable; CW, fast; FW, and slow; SW). The walking speeds performed experimentally were quantified as 1.28 ± 0.14 m/s (mean \pm standard deviation) for CW, 1.58 ± 0.09 m/s for FW (CW + 23%) and 0.86 ± 0.11 m/s for SW (CW - 33%). For every walking speed, five successful trials were assessed. A successful trial was obtained when a single foot hit one of the FPs entirely, followed by an entire hit of the other foot on the successive FP.

2.4. Overall description of the components in the musculoskeletal models

Three musculoskeletal models have been constructed in AnyBodyTM Modeling System (AMS) v.6.0.7 (AnyBodyTM Technology A/S, Aalborg, Denmark) [1]:

- a model in which the kinematics are driven by IMC and the GRF&M are predicted from the kinematics (IMC-PGRF).

- a model in which the kinematics are driven by OMC and the GRF&M are predicted from the kinematics (OMC-PGRF).
- a model in which the kinematics are driven by OMC and the GRF&M are measured from FPs (OMC-MGRF).

In the IMC-PGRF model, a Biovision Hierarchy (BVH) file is exported from Xsens MVN Studio and imported in AMS, in which a stick figure model is initially reconstructed. The BVH file contains a hierarchy part with a description of the linked segment model in a static pose, as well as a motion part that contains, for each time frame, the absolute position and orientation of the root pelvis segment, and the joint angles between the segments described in the hierarchy. The generated stick figure model contains 72 degrees-of-freedom (DOF). In order to match the stick figure model with the musculoskeletal model, we utilize a concept of virtual markers (VMs) demonstrated in a previous Kinect-based study [31]. The VMs are mapped to particular points of each model that are well defined in both models, such as joint centers and segment end points. The VM placement is illustrated in Figure 1 and described in more detail in the supplementary material. Following this step, the VMs are treated as actual experimental markers, as if they were derived from an OMC system and they are assigned weights in three directions in the segmentframe. Contrary to OMC, no filtering was applied to the VM trajectories.

In all models, the GaitFullBody template of the AnyBodyTM Managed Model Repository (AMMR) 1.6.2 was used to reconstruct the musculoskeletal models in AMS. The lumbar spine model was derived from the study of de Zee *et al.* [32], the lower limb model was derived from the Twente Lower Extremity Model Klein-Horsman *et al.* [33], and the shoulder and upper limb models were based on the model of the Delft Shoulder Group [34, 35, 36]. The full-body kinematic model contained 39 DOF in total. Specifically, a pelvis segment with three rotational and three translational DOF, two spherical hip joints, two revolute knee joints, two universal ankle joints, a spherical pelvic-lumbar joint, two glenohumeral joints with five DOF each, two universal elbow

169 joints, and two universal wrist joints. The motion of the neck joint was locked
170 to a neutral position.

171 2.5. Scaling and kinematics analysis of the musculoskeletal models

172 For each subject, a standing reference trial with an anatomical pose was
173 utilized to identify the parameters of segment lengths and the (virtual) marker
174 positions, using a least-square minimization between the model and input (vir-
175 tual or skin-mounted) marker positions [37]. In the IMC-PGRF musculoskeletal
176 model, the lengths of the shanks, thighs, head, upper arm and forearms were
177 derived directly from the stick figure, as generated from Xsens MVN studio us-
178 ing the measured body dimensions. In contrast, the pelvis width, foot length,
179 and trunk height were optimized based on the above-mentioned least-square
180 minimization method. The estimated segment lengths were used in all subse-
181 quent dynamic trials to perform the kinematic analysis based on the method of
182 Andersen *et al.* [38].

183 2.6. Inertial and geometric scaling of the musculoskeletal models

184 The mass of each segment was linearly scaled based on the total body mass
185 and the segment mass ratio values reported by Winter [4]. The inertial pa-
186 rameters were calculated by considering the segments as cylinders with uniform
187 density. In addition, geometric scaling of each segment, where the longitudinal
188 axis was defined as the second entry, was achieved using the following matrix:

$$S = \begin{bmatrix} \sqrt{\frac{m_s}{l_s}} & 0 & 0 \\ 0 & l_s & 0 \\ 0 & 0 & \sqrt{\frac{m_s}{l_s}} \end{bmatrix} \quad (1)$$

189 where S is the scaling matrix, l_s is the ratio between the unscaled and scaled
190 lengths of the segment, m_s is the mass ratio of the segment.

191 2.7. Muscle recruitment

192 The muscle recruitment problem was solved by defining an optimization
193 problem where a system of equations minimizes the cost function, subject to
194 the dynamic equilibrium equations and non-negativity constraints, so that each
195 muscle can only pull, but not push, while its force remains below its strength
196 [1, 31, 39].

197 The strengths of the muscles were derived from previous studies which de-
198 scribed the models of the body parts, and were considered constant for different
199 lengths and contraction velocities [32, 33, 34, 35, 36]. To scale the muscle
200 strengths, fat percentage was used as in Veeger *et al.* [35], calculated from the
201 body mass index [40]. The model of the lower body contained 110 muscles,
202 distributed into 318 individual muscle paths. In contrast, in the upper body
203 model, ideal joint torque generators were utilized. Actuators for residual forces
204 and moments with capacity up to 10 N and Nm, respectively, were placed at the
205 origin of the pelvis and included in the muscle recruitment problem previously
206 described.

207 2.8. Ground reaction force and moment prediction

208 The GRF&M were predicted by adjusting a method of Skals *et al.* [23]. A
209 set of eighteen dynamic contact points were overlaid 1 mm beneath the inferior
210 surface of each foot. Each dynamic contact point consisted of five unilateral
211 force actuators, which could generate a positive vertical force perpendicular to
212 the ground, and static friction forces in the anterior, posterior, medial, and
213 lateral directions using a friction coefficient of 0.5. In addition, the height and
214 velocity activation thresholds were set to 0.03 m and 1.2 m/s, respectively.

215 2.9. Data Analysis

216 Lower limb joint angles calculated in the IMC-PGRF model were compared
217 to the OMC-PGRF/OMC-MGRF. In addition, GRF&M and JRF&M of the
218 IMC-PGRF and OMC-PGRF were compared to OMC-MGRF.

Forces were normalized to body weight (BW) and moments to body weight times body height (BW*BH). The time axis of the curves was normalized to 100% of the gait cycle for the kinematics (time between two consecutive heel-strike events of the analyzed limb) and 100% of the stance phase (time between heel-strike and toe-off events of the analyzed limb) for the kinetics. Measured and estimated GRF&M were expressed on the right handed coordinate frame defined by the walking direction within the trial (given that the subjects walked straight) and the vertical axis equal to the vertical axis of the respective motion capture system used. On the other hand, JRF&M were expressed on the coordinate frame of the segment distal to the body in both IMC and OMC methods.

The above-mentioned comparisons of kinematic and kinetic variables to their respective references were performed using absolute and relative root-mean-square-differences (RMSD and rRMSD, respectively) as described by Ren *et al.* [19]. In addition, for every curve, the magnitude (M) and phase (P) difference metrics [41] have been utilized. Pearson correlation coefficient (ρ) were calculated, averaged using Fisher's z transformation method [42], and categorized similarly to Taylor *et al.* [43], as "weak" ($\rho \leq 0.35$), "moderate" ($0.35 < \rho \leq 0.67$), "strong" ($0.67 < \rho \leq 0.90$), and "excellent" ($\rho > 0.90$).

3. Results

3.1. Estimated kinematics of the musculoskeletal model

Table 1 presents the results for the accuracy analysis for the joint angles of the IMC-driven model versus the OMC-driven model. Similarly, Figure 2 illustrates the curves for the joint angles of the lower extremities averaged across all gait cycles performed by the eleven subjects. Excellent Pearson correlation coefficients have been found in all sagittal plane angles for ankle, knee, and hip (0.95, 0.99, and 0.99, respectively). For the same variables, the RMSDs across a gait cycle were found as $4.1 \pm 1.3^\circ$, $4.4 \pm 2.0^\circ$ and $5.7 \pm 2.1^\circ$, respectively (mean \pm standard deviation). Hip flexion angles were overall underestimated ($M =$

248 $-4.0 \pm 13.9\%$), whereas knee and ankle magnitude differences showed an average
 249 overestimation ($0.7 \pm 6.2\%$ and $8.6 \pm 16.4\%$). The hip abduction showed excellent
 250 correlations ($\rho = 0.91$) with an RMSD of $4.1 \pm 2.0^\circ$ and a mean underestimation
 251 with a magnitude difference $M = -12.2 \pm 34.7\%$. Strong correlation values ($\rho =$
 252 0.68) were observed in the hip internal-external rotation angle with an RMSD
 253 of $6.5 \pm 2.8^\circ$ and an underestimation of magnitude difference $M = 5.5 \pm 39.0\%$.
 254 Finally, the subtalar eversion angle showed strong correlation ($\rho = 0.82$), RMSD
 255 of $9.66 \pm 3.07^\circ$ and $M = 24.0 \pm 34.7\%$.

256 3.2. Predicted kinetics using inertial and optical motion capture

257 The results of the accuracy analysis for GRF&M and JRF&M are presented
 258 in Table 2 and 3, for IMC-PGRF and OMC-PGRF, respectively. The mean
 259 values and standard deviations of the curves from IMC-PGRF, OMC-PGRF,
 260 and OMC-MGRF models, are illustrated in Figures 3 and 4, for the forces and
 261 moments, respectively.

262 The Pearson correlation coefficients of the IMC-PGRF model were excellent
 263 for vertical ($\rho = 0.97$) and anteroposterior GRF&M ($\rho = 0.91$) and strong for
 264 mediolateral GRF&M ($\rho = 0.80$). For the same components, RMSD values
 265 observed were of 9.3 ± 3.0 , 5.5 ± 1.2 and 2.1 ± 0.6 %BW, respectively (mean
 266 \pm standard deviation). The OMC-PGRF model performed better in the an-
 267 teroposterior GRF&M components ($\rho = 0.96$, RMSD = 3.7 ± 1.1 %BW), and
 268 similarly to IMC-PGRF for the other two GRF&M components (mediolateral:
 269 $\rho = 0.79$, RMSD = 1.9 ± 0.5 BW, vertical: $\rho = 0.99$, RMSD = 5.9 ± 1.9 BW).

270 Concerning GRM, the sagittal plane was predicted with similar excellent
 271 correlations in both IMC-PGRF ($\rho = 0.91$) and OMC-PGRF ($\rho = 0.94$) driven
 272 models. The correlation coefficients for frontal and transverse GRM components
 273 found in the IMC-PGRF model were $\rho = 0.64$, $\rho = 0.82$, respectively, whereas
 274 in the OMC-PGRF model ($\rho = 0.66$, $\rho = 0.81$, respectively). The RMSDs
 275 found in the IMC-PGRF approach were 0.9 ± 0.6 , 1.6 ± 0.6 , and 0.2 ± 0.001
 276 %BW*BH for frontal, sagittal and transverse GR&M, respectively, which were
 277 either slightly higher or similar to the RMSDs of the OMC-PGRF approach

(0.7 ± 0.2 , 1.2 ± 0.4 , and 0.2 ± 0.1 %BW*BH, respectively).

4. Discussion

We have presented a method to perform musculoskeletal model-based inverse dynamics using exclusively IMC input (IMC-PGRF). First, we compared the kinematic joint angle estimates of the lower limbs against those assessed through a conventional, laboratory-based OMC input. In addition, we tested the performance of the approach in calculating the JRF&M, while predicting the GRF&M from the kinematics, against a similarly constructed model (OMC-MGRF) which uses input from both FP and OMC. Finally, we performed a similar comparison to evaluate the predicted kinetics of a model driven exclusively by OMC input (OMC-PGRF).

Regarding the IMC-based joint angles in the musculoskeletal model, all three sagittal plane angles provided excellent correlations (range: 0.95-0.99) and average RMSD values remained below 6° . Slightly lower correlations were observed in the frontal and transverse plane angles, which can be explained due to the smaller range of motion within these planes. For instance, even though the hip abduction and external rotation joint angles present absolute RMSD values similar to the flexion component, their rRMSDs which take into account the range of motion are two and three times higher, respectively.

Both GRF&M and JRF&M of the vertical axis presented higher correlations and lower RMSDs than the ones in the anteroposterior and mediolateral axes. Similarly, sagittal plane moments were found in most cases to be more accurate than frontal and transverse plane moments. By visual inspection of the curves, we observe that the magnitude of the IMC-PGRF anteroposterior GRF&M seems to be underestimated both in the negative early stance and positive late stance peak, which can be confirmed by the magnitude difference for that curve ($M = -28.3\%$). However, this behaviour is not observed in the OMC-PGRF, nor during the single stance of the IMC-PGRF curve. Despite the higher rRMSD found in the non-sagittal joint angles, the performance of the IMC-PGRF in

the mediolateral, frontal and transverse plane GRF&M components matched closely the OMC-PGRF approach. This observation reveals that OMC-based kinematics suffer from errors of similar size, when capturing the typically small movements of the frontal and transverse planes, given the fact that both IMC-PGRF and OMC-PGRF had the same model characteristics. Therefore, OMC-MGRF should also be used with caution, when comparing either kinematic or JRF&M quantities of the non-sagittal planes.

A number of error sources contribute to discrepancies in the OMC kinematics. First, soft tissue artefacts can create a relative movement of the marker with respect to the bone [44, 45]. In addition, mismatches between the experimental and modelled marker positions can lead to errors in segment orientations calculated during inverse kinematics. Both error sources would have a relatively larger impact on the kinematics of the frontal and transverse plane, than on the sagittal plane. Finally, the JRF&M of the OMC-PGRF were compared against a non-independent OMC-MGRF reference, which could have contributed to underestimation of the actual errors.

The IMC-PGRF approach has a number of possible sources of errors which would influence the performance. Similarly to OMC models, soft-tissue artefacts may compromise the kinematic estimates. Further errors in segment kinematics may stem due to the N-pose calibration assumptions. In particular, mismatches between the practised and modelled N-pose could result in offsets in the estimated positions. Other common error sources in IMC include manual measurements of segment lengths as well as IMU inaccuracies. In addition, the stick figure model, which was utilized to recreate the VMs, has a higher number of DOF, compared to the musculoskeletal model used.

A possible source of error in all inverse dynamic approaches concerns the inertial parameters (masses and moments of inertia), as well as the center of mass (CoM) locations of each human body segment, which were calculated based on anthropometric tables found in the literature.

This study focused on presenting and evaluating a general workflow for musculoskeletal model-based inverse dynamic simulations using ambulatory IMC

338 systems. The presentation of results in this study was performed on the level of
339 ground and joint reaction forces and moments. These measures are calculated
340 from muscle force estimates derived from a muscle recruitment optimization
341 technique. Given the high number of muscles in the model (110) and without
342 a clear medical research question, it is challenging to choose which muscles are
343 more important to present and analyze. Future studies could examine specific
344 applications and pathologies in order to identify the most important muscles
345 and evaluate their respective force estimates.

346 A limitation of this study is that, even though the method has been pre-
347 viously shown to be universally applicable in OMC-based studies [22, 23], we
348 only evaluated its performance in gait of three different speeds. In addition,
349 our experiments included only young healthy male subjects, but the underlying
350 methods to predict kinetics from kinematics have been recently shown to be
351 applicable in Parkinson's patients [46]. Future studies could investigate the ap-
352 plication of IMC systems combined with musculoskeletal modeling in groups of
353 larger sample size than the current study, including patients, as well as female
354 subjects.

355 5. Conclusion

356 In this study, we have demonstrated a workflow to perform musculoskeletal
357 model-based inverse dynamics using input from a commercially available IMC
358 system. Our validation findings indicate that the prediction of GRF&M as well
359 as JRF&M using musculoskeletal model-based inverse dynamics based on only
360 IMC data provides comparable performance to both OMC-PGRF and OMC-
361 MGRF methods. The proposed method allows assessment of kinetic variables
362 outside the laboratory.

363 Ethical approval

364 The ethical guidelines of The Scientific Ethical Committee for the Region of
365 North Jutland (Den Videnskabetiske Komit for Region Nordjylland) were fol-

lowed and all volunteers signed written informed consent after receiving detailed information prior to data collection.

Conflict of interest statement

Three of the authors are employees of Xsens Technologies B.V. that manufactures and sells the Xsens MVN. One of the authors is employee of AnyBody Technology A/S that owns and sells the AnyBody Modeling System.

Acknowledgements

This study was performed in the context of KNEEMO Initial Training Network, funded by the European Unions Seventh Framework Programme for research, technological development, and demonstration under Grant Agreement No. 607510 (www.kneemo.eu). This work was also supported by the Danish Council for Independent Research under grant no. DFF-4184-00018 to M. S. Andersen. Finally, this research received funding in part from the European Unions Horizon 2020 research and innovation programme under grant agreement No. 680754 (The MovAiD project, www.movaid.eu).

References

References

- [1] M. Damsgaard, J. Rasmussen, S. T. Christensen, E. Surma, M. de Zee, Analysis of musculoskeletal systems in the anybody modeling system, *Simulation Modelling Practice and Theory* 14 (2006) 1100–1111.
- [2] S. L. Delp, F. C. Anderson, A. S. Arnold, P. Loan, A. Habib, C. T. John, E. Guendelman, D. G. Thelen, Opensim: Open-source software to create and analyze dynamic simulations of movement, *IEEE Transactions on Biomedical Engineering* 54 (2007) 1940–1950. doi:10.1109/TBME.2007.901024.
- [3] A. Erdemir, S. McLean, W. Herzog, A. J. van den Bogert, Model-based estimation of muscle forces exerted during movements, *Clinical Biomechanics* 22 (2007) 131 – 154. doi:https://doi.org/10.1016/j.clinbiomech.2006.09.005.
- [4] D. A. Winter, *Biomechanics and Motor Control of Human Movement* (1990).
- [5] J. Rasmussen, M. Damsgaard, M. Voigt, Muscle recruitment by the min/max criterion - a comparative numerical study, *Journal of Biomechanics* 34 (2001) 409–415. doi:10.1016/S0021-9290(00)00191-3.
- [6] J. H. Challis, The variability in running gait caused by force plate targeting, *Journal of Applied Biomechanics* 17 (2001) 77–83.
- [7] R. Riemer, E. T. Hsiao-Wecksler, X. Zhang, Uncertainties in inverse dynamics solutions: A comprehensive analysis and an application to gait, *Gait and Posture* 27 (2008) 578–588. doi:10.1016/j.gaitpost.2007.07.012.
- [8] H. Hatze, The fundamental problem of myoskeletal inverse dynamics and its implications, *Journal of Biomechanics* 35 (2002) 109–115. doi:10.1016/S0021-9290(01)00158-0.

- [9] P. H. Veltink, C. Liedtke, E. Droog, H. Van Der Kooij, Ambulatory measurement of ground reaction forces, *IEEE Transactions on Neural Systems and Rehabilitation Engineering* 13 (2005) 423–427. doi:10.1109/TNSRE.2005.847359.
- [10] H. M. Schepers, H. F. J. M. Koopman, P. H. Veltink, Ambulatory assessment of ankle and foot dynamics, *IEEE Transactions on Biomedical Engineering* 54 (2007) 895–902. doi:10.1109/TBME.2006.889769.
- [11] T. Liu, Y. Inoue, K. Shibata, A wearable force plate system for the continuous measurement of triaxial ground reaction force in biomechanical applications, *Measurement Science and Technology* 21 (2010). doi:10.1088/0957-0233/21/8/085804.
- [12] A. Forner Cordero, H. J. F. M. Koopman, F. C. T. Van Der Helm, Use of pressure insoles to calculate the complete ground reaction forces, *Journal of Biomechanics* 37 (2004) 1427–1432. doi:10.1016/j.jbiomech.2003.12.016.
- [13] H. Rouhani, J. Favre, X. Crevoisier, K. Aminian, Ambulatory assessment of 3d ground reaction force using plantar pressure distribution, *Gait and Posture* 32 (2010) 311–316. doi:10.1016/j.gaitpost.2010.05.014.
- [14] Y. Jung, M. Jung, K. Lee, S. Koo, Ground reaction force estimation using an insole-type pressure mat and joint kinematics during walking, *Journal of Biomechanics* 47 (2014) 2693–2699. doi:10.1016/j.jbiomech.2014.05.007.
- [15] J. Van Den Noort, M. Van Der Esch, M. P. Steultjens, J. Dekker, H. M. Schepers, P. H. Veltink, J. Harlaar, Influence of the instrumented force shoe on gait pattern in patients with osteoarthritis of the knee, *Medical and Biological Engineering and Computing* 49 (2011) 1381–1392. doi:10.1007/s11517-011-0818-z.

- [16] C. Liedtke, S. A. W. Fokkenrood, J. T. Menger, H. van der Kooij, P. H. Veltink, Evaluation of instrumented shoes for ambulatory assessment of ground reaction forces, *Gait and Posture* 26 (2007) 39–47. doi:10.1016/j.gaitpost.2006.07.017.
- [17] D. C. Low, S. J. Dixon, Footscan pressure insoles: Accuracy and reliability of force and pressure measurements in running, *Gait and Posture* 32 (2010) 664–666. doi:10.1016/j.gaitpost.2010.08.002.
- [18] M. L. Audu, R. F. Kirsch, R. J. Triolo, Experimental verification of a computational technique for determining ground reactions in human bipedal stance, *Journal of Biomechanics* 40 (2007) 1115–1124. doi:10.1016/j.jbiomech.2006.04.016.
- [19] L. Ren, R. K. Jones, D. Howard, Whole body inverse dynamics over a complete gait cycle based only on measured kinematics, *Journal of Biomechanics* 41 (2008) 2750–2759. doi:10.1016/j.jbiomech.2008.06.001.
- [20] S. E. Oh, A. Choi, J. H. Mun, Prediction of ground reaction forces during gait based on kinematics and a neural network model, *Journal of Biomechanics* 46 (2013) 2372–2380. doi:10.1016/j.jbiomech.2013.07.036.
- [21] A. Choi, J.-M. Lee, J. H. Mun, Ground reaction forces predicted by using artificial neural network during asymmetric movements, *International Journal of Precision Engineering and Manufacturing* 14 (2013) 475–483. doi:10.1007/s12541-013-0064-4.
- [22] R. Fluit, M. S. Andersen, S. Kolk, N. Verdonschot, H. F. J. M. Koopman, Prediction of ground reaction forces and moments during various activities of daily living, *Journal of Biomechanics* 47 (2014) 2321–2329. doi:10.1016/j.jbiomech.2014.04.030.
- [23] S. Skals, M. Jung, M. Damsgaard, M. S. Andersen, Prediction of ground reactions forces and moments during sports-related movements, *Multibody Syst. Dyn* (2016).

- [24] H. J. Luinge, P. H. Veltink, Measuring orientation of human body segments using miniature gyroscopes and accelerometers, *Medical and Biological Engineering and Computing* 43 (2005) 273–282. doi:10.1007/BF02345966.
- [25] D. Roetenberg, H. J. Luinge, C. T. M. Baten, P. H. Veltink, Compensation of magnetic disturbances improves inertial and magnetic sensing of human body segment orientation, *IEEE Transactions on Neural Systems and Rehabilitation Engineering* 13 (2005) 395–405. doi:10.1109/TNSRE.2005.847353.
- [26] D. Roetenberg, H. Luinge, P. Slycke, M. Xsens, Full 6DOF Human Motion Tracking Using Miniature Inertial Sensors (2009).
- [27] J.-T. Zhang, A. C. Novak, B. Brouwer, Q. Li, Concurrent validation of xsens mvn measurement of lower limb joint angular kinematics, *Physiological Measurement* 34 (2013) N63–N69. doi:10.1088/0967-3334/34/8/N63.
- [28] A. Karatsidis, G. Bellusci, H. M. Schepers, M. de Zee, M. S. Andersen, P. H. Veltink, Estimation of ground reaction forces and moments during gait using only inertial motion capture, *Sensors (Switzerland)* 17 (2017). doi:10.3390/s17010075.
- [29] B. H. W. Koning, M. M. van der Krogt, C. T. M. Baten, B. F. J. M. Koopman, Driving a musculoskeletal model with inertial and magnetic measurement units, *Computer Methods in Biomechanics and Biomedical Engineering* 18 (2015) 1003–1013. doi:10.1080/10255842.2013.867481.
- [30] Xsens, Mvn user manual by xsens mvn - issuu, http://issuu.com/xsensmvn/docs/mvn_user_manual_71c37181653db5?e=14522406/12478179, 2017. (Accessed on 02/03/2018).
- [31] S. Skals, K. Rasmussen, K. Bendtsen, J. Yang, M. Andersen, A musculoskeletal model driven by dual microsoft kinect sensor data, *Multibody System Dynamics* (2017). doi:10.1007/s11044-017-9573-8.

- [32] M. de Zee, L. Hansen, C. Wong, J. Rasmussen, E. B. Simonsen, A generic detailed rigid-body lumbar spine model, *Journal of Biomechanics* 40 (2007) 1219–1227. doi:10.1016/j.jbiomech.2006.05.030.
- [33] M. D. Klein Horsman, H. F. J. M. Koopman, F. C. T. van der Helm, L. P. Pros, H. E. J. Veeger, Morphological muscle and joint parameters for musculoskeletal modelling of the lower extremity, *Clinical Biomechanics* 22 (2007) 239–247. doi:10.1016/j.clinbiomech.2006.10.003.
- [34] H. E. J. Veeger, F. C. T. Van Der Helm, L. H. V. Van Der Woude, G. M. Pronk, R. H. Rozendal, Inertia and muscle contraction parameters for musculoskeletal modelling of the shoulder mechanism, *Journal of Biomechanics* 24 (1991) 615–629. doi:10.1016/0021-9290(91)90294-W.
- [35] H. E. J. Veeger, B. Yu, K.-N. An, R. H. Rozendal, Parameters for modeling the upper extremity, *Journal of Biomechanics* 30 (1997) 647–652. doi:10.1016/S0021-9290(97)00011-0.
- [36] F. C. T. Van der Helm, H. E. J. Veeger, G. M. Pronk, L. H. V. Van der Woude, R. H. Rozendal, Geometry parameters for musculoskeletal modelling of the shoulder system, *Journal of Biomechanics* 25 (1992) 129–144. doi:10.1016/0021-9290(92)90270-B.
- [37] M. S. Andersen, M. Damsgaard, B. MacWilliams, J. Rasmussen, A computationally efficient optimisation-based method for parameter identification of kinematically determinate and over-determinate biomechanical systems, *Computer Methods in Biomechanics and Biomedical Engineering* 13 (2010) 171–183. doi:10.1080/10255840903067080.
- [38] M. S. Andersen, M. Damsgaard, J. Rasmussen, Kinematic analysis of over-determinate biomechanical systems, *Computer Methods in Biomechanics and Biomedical Engineering* 12 (2009) 371–384. doi:10.1080/10255840802459412.

- [39] M. A. Marra, V. Vanheule, R. Fluit, B. H. F. J. M. Koopman, J. Rasmussen, N. Verdonchot, M. S. Andersen, A subject-specific musculoskeletal modeling framework to predict in vivo mechanics of total knee arthroplasty, *Journal of Biomechanical Engineering* 137 (2015). doi:10.1115/1.4029258.
- [40] D. C. Frankenfield, W. A. Rowe, R. N. Cooney, J. S. Smith, D. Becker, Limits of body mass index to detect obesity and predict body composition, *Nutrition* 17 (2001) 26–30. doi:10.1016/S0899-9007(00)00471-8.
- [41] M. A. Sprague, T. L. Geers, Spectral elements and field separation for an acoustic fluid subject to cavitation, *Journal of Computational Physics* 184 (2003) 149–162. doi:10.1016/S0021-9991(02)00024-4.
- [42] N. C. Silver, W. P. Dunlap, Averaging correlation coefficients: should fisher's z transformation be used?, *Journal of Applied Psychology* 72 (1987) 146.
- [43] R. Taylor, Interpretation of the correlation coefficient: A basic review, *Journal of Diagnostic Medical Sonography* 6 (1990) 35–39. doi:10.1177/875647939000600106.
- [44] L. Chiari, U. D. Croce, A. Leardini, A. Cappozzo, L. Chiari, U. D. Croce, A. Cappozzo, U. Della Croce, A. Leardini, L. Chiari, Human movement analysis using stereophotogrammetry, *Gait Posture* 21 (2005) 226–237.
- [45] A. Leardini, A. Chiari, U. Della Croce, A. Cappozzo, Human movement analysis using stereophotogrammetry part 3. soft tissue artifact assessment and compensation, *Gait and Posture* 21 (2005) 212–225. doi:10.1016/j.gaitpost.2004.05.002.
- [46] M. Eltoukhy, C. Kuenze, M. S. Andersen, J. Oh, J. Signorile, Prediction of ground reaction forces for parkinson's disease patients using a kinect-driven musculoskeletal gait analysis model, *Medical Engineering & Physics*

544 50 (2017) 75–82. URL: [https://doi.org/10.1016/j.medengphy.2017.](https://doi.org/10.1016/j.medengphy.2017.10.004)
545 10.004. doi:10.1016/j.medengphy.2017.10.004.

Accepted manuscript

546 List of Figures

547	1	Illustration of the pipeline used in the IMC-PGRF approach. A	
548		recording from Xsens MVN Studio (a) is exported to a BVH	
549		file to generate a stick figure model (b), in which virtual markers	
550		(blue) are placed. Virtual markers (red) are also placed on points	
551		of the musculoskeletal model (c), and by projecting b on c the	
552		kinematics of the musculoskeletal model are solved. Finally, in-	
553		verse dynamic analysis using prediction of ground reaction forces	
554		and moments is performed to estimate the kinetics.	24
555	2	Ankle, knee, and hip joint angle estimates (standard deviation	
556		around mean) of the IMC-PGRF (orange shaded area around	
557		orange dotted line) and OMC-PGRF models (blue shaded area	
558		around blue dashed line) versus OMC-MGRF model (thin black	
559		solid lines around thick black solid line).	25
560	3	Ground and lower limb joint reaction force estimates (standard	
561		deviation around mean) of the IMC-PGRF (orange shaded area	
562		around orange dotted line) and OMC-PGRF models (blue shaded	
563		area around blue dashed line) versus OMC-MGRF model (thin	
564		black solid lines around thick black solid line).	26
565	4	Ground reaction and lower limb net joint moment estimates (stan-	
566		dard deviation around mean) of the IMC-PGRF (orange shaded	
567		area around orange dotted line) and OMC-PGRF models (blue	
568		shaded area around blue dashed line) versus OMC-MGRF model	
569		(thin black solid lines around thick black solid line).	27

Figure 1

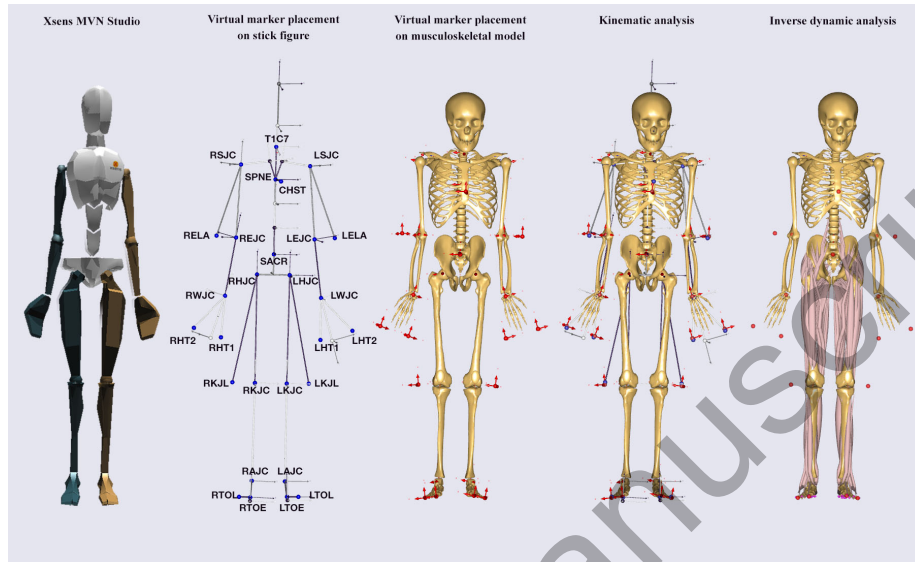
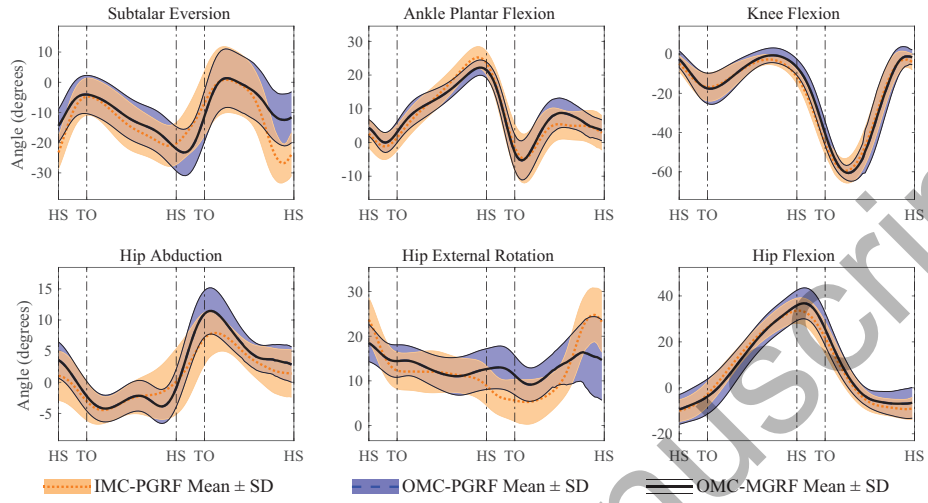


Figure 2



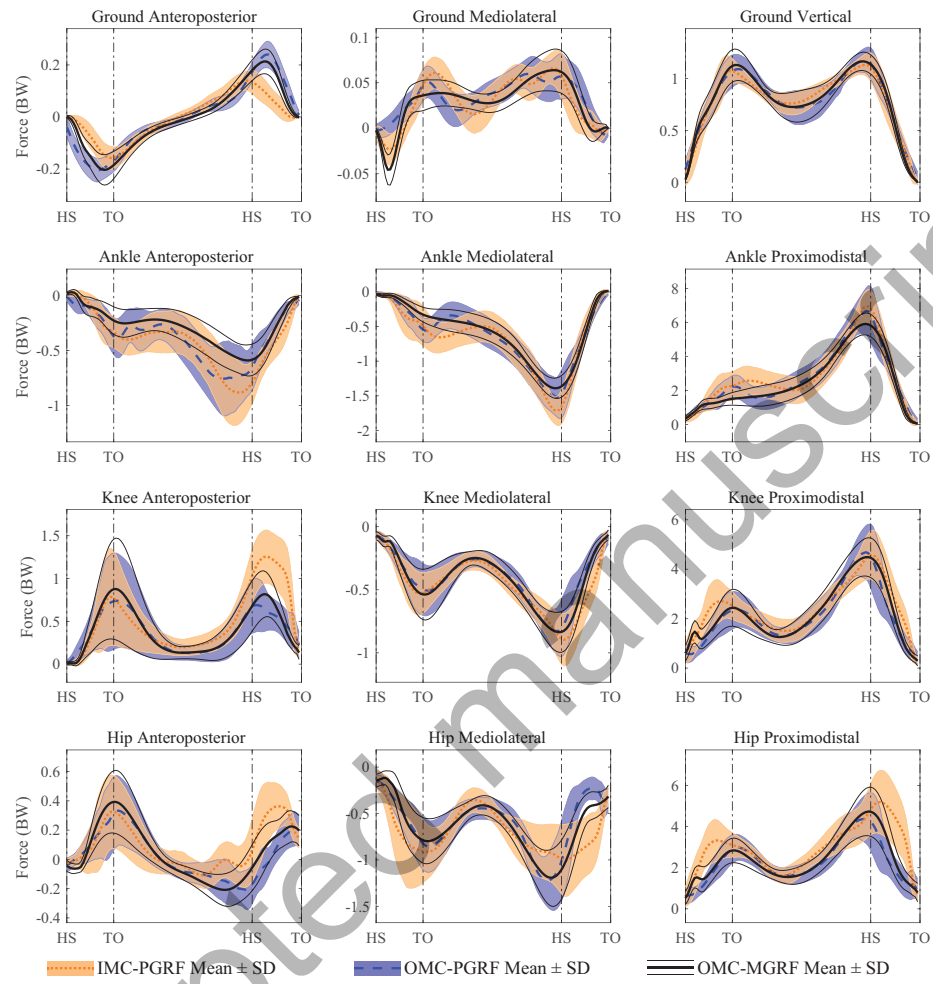


Figure 3

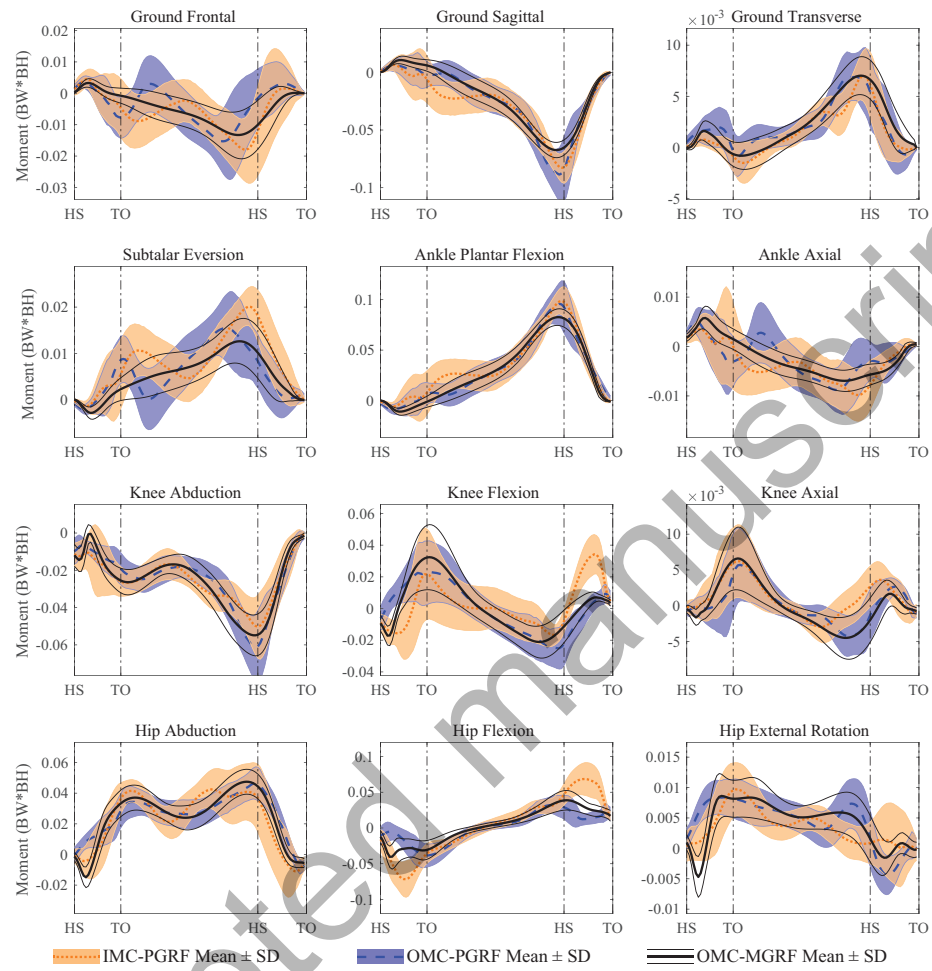


Figure 4

570 **List of Tables**

571	1	Comparison of lower limb joint angles between musculoskeletal model driven by the inertial (IMC-PGRF) and optical motion capture (OMC-PGRF/OMC-MGRF), using Pearson correlation coefficient (ρ), absolute and relative root-mean-squared-differences ($RMSD$ in degrees and $rRMSD$ in %, respectively). M and P denote the % magnitude and phase differences	29
572			
573			
574			
575			
576			
577	2	IMC-PGRF-based ground and joint reaction forces (first three quantities) and net moments (second three quantities) versus OMC-MGRF. Pearson correlation coefficient is denoted with ρ . Absolute per body weight (or body weight times height) and relative root-mean-squared-difference are denoted with $RMSD$ (%BW or %BW*BH) and $rRMSD$ (%), respectively. M and P indicate the magnitude and phase differences (%).	30
578			
579			
580			
581			
582			
583			
584	3	OMC-PGRF-based ground and joint reaction forces (first three quantities) and net moments (second three quantities) versus OMC-MGRF. Pearson correlation coefficient is denoted with ρ . Absolute per body weight (or body weight times height) and relative root-mean-squared-difference are denoted with $RMSD$ (%BW or %BW*BH) and $rRMSD$ (%), respectively. M and P indicate the magnitude and phase differences (%).	31
585			
586			
587			
588			
589			
590			

Table 1

	ρ	RMSD	rRMSD	M	P
Subtalar Eversion	0.81	9.7 (3.2)	32.6 (10.3)	24.0 (34.7)	19.3 (10.2)
Ankle Plantarflexion	0.95	4.1 (1.3)	14.0 (4.8)	8.6 (16.4)	9.8 (3.9)
Knee Flexion	0.99	4.4 (2.0)	7.2 (3.4)	0.7 (6.2)	4.8 (2.7)
Hip Abduction	0.91	4.1 (2.0)	25.9 (10.7)	-12.2 (34.7)	21.2 (9.3)
Hip External Rotation	0.68	6.5 (2.8)	36.9 (15.2)	5.5 (39.0)	12.6 (6.2)
Hip Flexion	0.99	5.7 (2.1)	12.7 (5.3)	-4.0 (13.9)	8.8 (4.2)

Table 2

	ρ	RMSD	rRMSD	M	P
Ground					
Anteroposterior	0.91	5.5 (1.2)	15.0 (2.4)	-25.4 (7.3)	14.4 (3.2)
Mediolateral	0.80	2.1 (0.6)	18.5 (3.2)	7.3 (19.3)	15.4 (3.8)
Vertical	0.97	9.3 (3.0)	7.7 (2.1)	-1.5 (1.5)	3.4 (1.0)
Frontal	0.64	0.9 (0.6)	38.0 (23.1)	125.5 (319.9)	30.6 (17.3)
Sagittal	0.91	1.6 (0.6)	17.5 (6.8)	14.3 (18.2)	12.1 (4.5)
Transverse	0.82	0.2 (0.1)	23.3 (7.2)	-8.5 (41.9)	17.8 (5.3)
Ankle					
Anteroposterior	0.84	22.2 (10.3)	26.1 (10.2)	49.0 (45.8)	10.8 (2.1)
Mediolateral	0.93	24.3 (8.9)	15.2 (5.3)	14.3 (17.1)	7.9 (2.7)
Proximodistal	0.93	88.5 (30.6)	13.6 (4.6)	9.8 (14.1)	7.2 (2.3)
Eversion	0.76	0.6 (0.2)	33.3 (20.2)	107.7 (220.3)	18.9 (10.7)
Plantar Flexion	0.93	1.6 (0.6)	15.1 (6.6)	10.6 (18.1)	9.9 (3.6)
Axial	0.67	0.5 (0.2)	30.4 (12.2)	46.5 (49.1)	27.2 (13.5)
Knee					
Anteroposterior	0.82	30.6 (10.3)	25.8 (9.7)	43.7 (53.5)	13.0 (4.5)
Mediolateral	0.91	12.0 (3.5)	14.1 (3.8)	6.6 (8.6)	7.0 (2.0)
Proximodistal	0.90	63.1 (26.9)	14.3 (6.6)	5.1 (9.1)	7.2 (2.8)
Abduction	0.81	1.1 (0.4)	18.9 (6.8)	-2.7 (16.1)	10.7 (3.8)
Flexion	0.58	1.9 (0.5)	29.8 (7.6)	17.9 (45.0)	32.8 (9.6)
Axial	0.73	0.3 (0.1)	25.4 (10.3)	2.3 (30.5)	27.9 (13.8)
Hip					
Anteroposterior	0.71	17.6 (7.6)	27.2 (9.6)	6.8 (24.4)	27.6 (10.9)
Mediolateral	0.73	27.0 (12.5)	23.0 (7.4)	7.7 (14.6)	10.6 (4.1)
Proximodistal	0.78	102.8 (30.6)	21.7 (4.5)	20.2 (10.0)	9.0 (2.5)
Abduction	0.83	1.4 (0.7)	19.7 (5.8)	6.3 (16.9)	13.7 (7.9)
Flexion	0.92	2.2 (0.6)	19.4 (4.2)	73.2 (26.3)	14.8 (4.2)
External Rotation	0.50	0.5 (0.2)	31.6 (6.6)	-3.9 (36.4)	25.6 (10.1)

Table 3

	ρ	RMSD	rRMSD	M	P
Ground					
Anteroposterior	0.96	3.7 (1.1)	8.3 (2.0)	7.7 (12.0)	8.8 (1.8)
Mediolateral	0.79	1.9 (0.5)	18.6 (4.1)	2.4 (10.8)	15.2 (4.9)
Vertical	0.99	5.9 (1.9)	4.9 (1.4)	-1.2 (1.1)	2.1 (0.7)
Frontal	0.66	0.7 (0.2)	30.3 (9.3)	71.0 (122.2)	24.5 (9.1)
Sagittal	0.94	1.2 (0.4)	13.1 (3.8)	15.9 (15.3)	9.2 (3.2)
Transverse	0.81	0.2 (0.1)	20.7 (7.5)	7.1 (22.9)	17.5 (7.5)
Ankle					
Anteroposterior	0.83	18.9 (6.9)	23.0 (6.1)	37.3 (28.6)	10.8 (2.3)
Mediolateral	0.96	16.1 (4.2)	10.7 (2.6)	6.8 (9.6)	5.8 (2.1)
Proximodistal	0.96	62.2 (17.6)	9.8 (2.7)	7.1 (9.0)	5.2 (1.8)
Eversion	0.76	0.5 (0.1)	25.5 (7.0)	45.3 (64.1)	18.7 (10.2)
Plantar Flexion	0.96	1.0 (0.3)	10.1 (3.3)	5.9 (10.0)	7.0 (2.6)
Axial	0.64	0.5 (0.1)	27.2 (7.3)	33.3 (36.9)	27.5 (11.5)
Knee					
Anteroposterior	0.93	11.9 (4.5)	12.3 (4.3)	-7.3 (8.7)	7.4 (2.0)
Mediolateral	0.96	7.2 (2.0)	8.8 (2.6)	-4.2 (5.6)	4.4 (1.0)
Proximodistal	0.95	41.7 (12.0)	9.3 (2.6)	-2.7 (5.8)	4.9 (1.2)
Abduction	0.91	0.8 (0.2)	12.6 (2.6)	-0.1 (10.5)	7.7 (1.6)
Flexion	0.86	0.9 (0.3)	16.7 (4.8)	-1.7 (14.3)	16.9 (5.2)
Axial	0.82	0.2 (0.1)	18.5 (6.6)	-3.4 (17.7)	20.6 (8.0)
Hip					
Anteroposterior	0.89	9.9 (3.6)	16.0 (6.7)	-10.4 (10.6)	16.6 (7.6)
Mediolateral	0.92	14.7 (4.0)	12.7 (3.1)	-1.9 (6.9)	6.2 (1.5)
Proximodistal	0.92	50.0 (15.9)	11.5 (2.6)	-4.6 (6.1)	5.5 (1.2)
Abduction	0.91	0.8 (0.2)	13.3 (2.6)	-3.2 (6.3)	8.7 (2.4)
Flexion	0.86	1.3 (0.4)	16.4 (3.4)	-9.3 (12.3)	18.0 (4.1)
External Rotation	0.68	0.3 (0.1)	22.5 (3.7)	6.5 (15.8)	18.8 (4.8)

Supplementary material

Title:

Musculoskeletal model-based inverse dynamic analysis under ambulatory conditions using inertial motion capture

Authors:

Angelos Karatsidis^{1,2}, Moonki Jung³, H. Martin Schepers¹, Giovanni Bellusci¹, Mark de Zee⁴, Peter H. Veltink², Michael Skipper Andersen⁵

Affiliations:

¹Xsens Technologies B.V., Enschede 7521 PR, The Netherlands

²Institute for Biomedical Technology and Technical Medicine (MIRA), University of Twente, Enschede 7500 AE, The Netherlands

³AnyBody Technology A/S, Aalborg 9220, Denmark

⁴Department of Health Science and Technology, Aalborg University, Aalborg 9220, Denmark

⁵Department of Materials and Production, Aalborg University, Aalborg 9220, Denmark

Corresponding author:

Angelos Karatsidis, Address: Xsens Technologies B.V., Enschede 7521 PR, The Netherlands, E-mail: angelos.karatsidis@xsens.com, Tel.: +31 88 97367 36, Fax: +31 88 97367 01

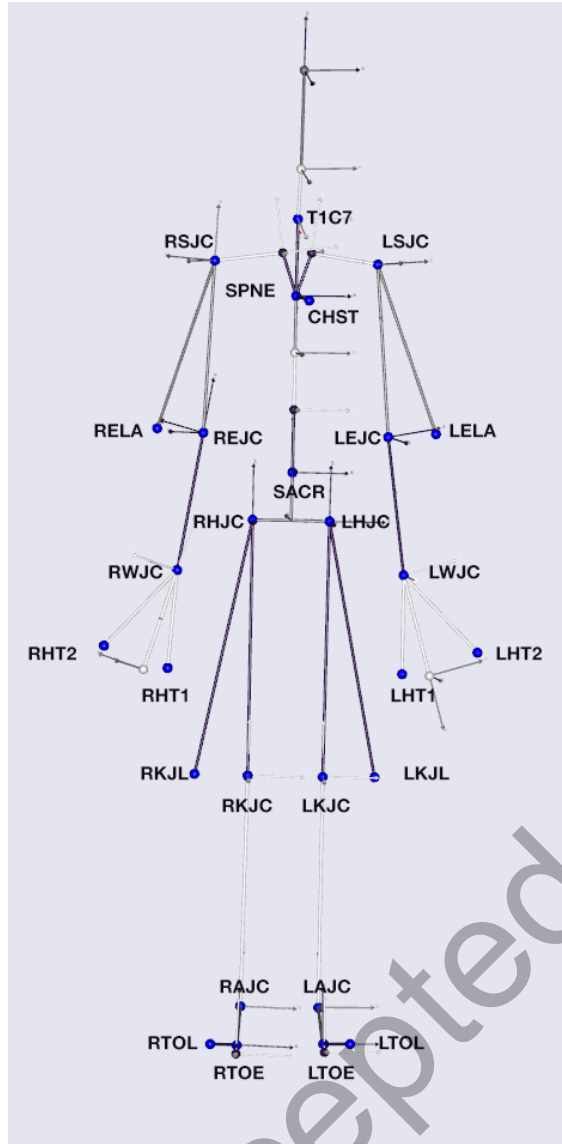
Keywords:

musculoskeletal modeling, inertial motion capture, inverse dynamics, ground reaction forces and moments, gait analysis

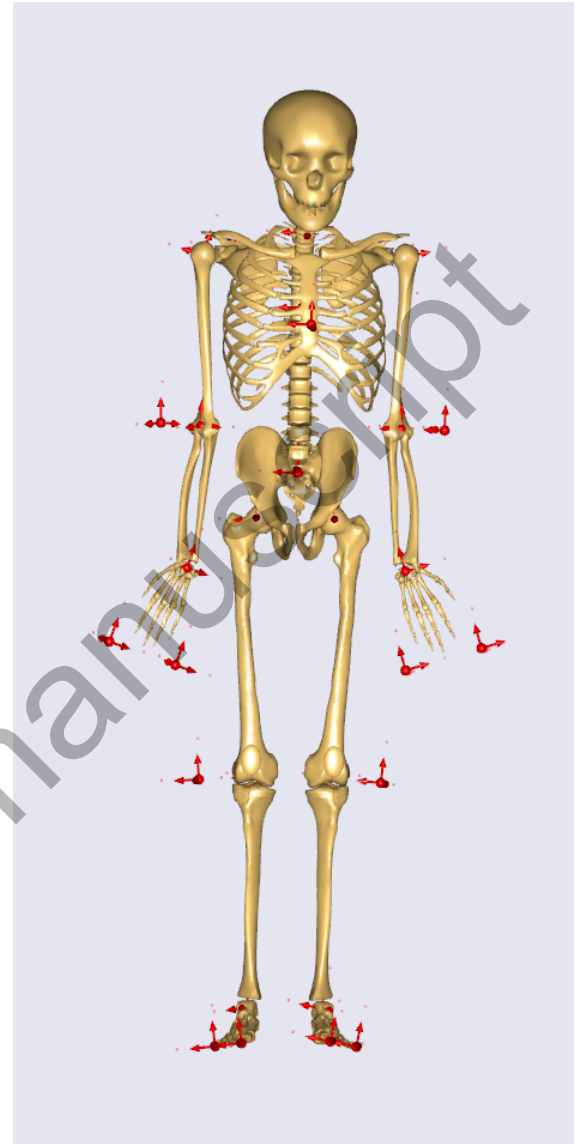
1. Virtual marker placement

Table 1: Description of the placement of virtual markers (VM) on the segments of the Xsens MVN model (stick figure model) and the musculoskeletal model constructed based on the AnyBody Managed Model Repository (AMMR).

VM Name	VM Placement on MVN	VM Placement on AMMR	VM Weight
T1C7	jT1C7	T1/C7 Joint	(1,1,1)
SPNE	jT9T8	Inferior to T1/C7 Joint	(1,1,1)
CHST	Anterior to jT9T8	Inferior and Anterior to T1/C7 Joint	(1,1,1)
SACR	jL5S1	Anterior to Pelvis/Sacrum Joint	(10,0,0)
RHJC	jRightHip	Right Hip Joint	(10,10,10)
RKJC	jRightKnee	Right Knee Joint	(2,2,2)
RKJL	Lateral to jRightKnee	Lateral to Right Knee Joint	(1,0,0)
RAJC	jRightAnkle	Right Ankle Joint	(1,1,1)
RTOE	jRightBallFoot	Right Big Toe Node	(1,1,1)
RTOL	Lateral to jRightBallFoot	Lateral to Right Big Toe Node	(0,1,0)
RSJC	jRightShoulder	Right Glenohumeral Joint	(0,2,2)
REJC	jRightElbow	Elbow Joint	(2,2,2)
RELA	Lateral to jRightElbow	Lateral to Elbow Joint	(1,1,1)
RWJC	jRightWrist	Right Wrist Joint	(2,2,2)
RHT1	Inferior and Medial to jRightWrist	Inferior and Medial to Right Wrist Joint	(0.5,0.5,0.5)
RHT2	Inferior and Lateral to jRightWrist	Inferior and Lateral to Right Wrist Joint	(0.5,0.5,0.5)
LHJC	jLeftHip	Left Hip Joint	(10,10,10)
LKJC	jLeftKnee	Left Knee Joint	(2,2,2)
LKJL	Lateral to jLeftKnee	Lateral to Left Knee Joint	(1,0,0)
LAJC	jLeftAnkle	Left Ankle Joint	(1,1,1)
LTOE	jLeftBallFoot	Left Big Toe Node	(1,1,1)
LTOL	Lateral to jLeftBallFoot	Lateral to Left Big Toe Node	(0,1,0)
LSJC	jLeftShoulder	Left Glenohumeral Joint	(0,2,2)
LEJC	jLeftElbow	Elbow Joint	(2,2,2)
LELA	Lateral to jLeftElbow	Lateral to Elbow Joint	(1,1,1)
LWJC	jLeftWrist	Left Wrist Joint	(2,2,2)
LHT1	Inferior and Medial to jLeftWrist	Inferior and Medial to Left Wrist Joint	(0.5,0.5,0.5)
LHT2	Inferior and Lateral to jLeftWrist	Inferior and Lateral to Left Wrist Joint	(0.5,0.5,0.5)



(a) Xsens MVN (stick-figure) model



(b) AnyBody Musculoskeletal Model (AMMR)

Figure 1: Illustration of the placement of the virtual markers (VM) on the segments of the Xsens MVN model (stick figure model) and the musculoskeletal model constructed based on the AnyBody Managed Model Repository (AMMR).

2. Accuracy analysis per walking speed

2.1. Comfortable walking speed

Table 2: Comfortable walking speed; comparison of lower limb joint angles between musculoskeletal model driven by the inertial (IMC-PGRF) and optical motion capture (OMC-PGRF/OMC-MGRF), using Pearson correlation coefficient (ρ), absolute and relative root-mean-squared-differences ($RMSD$ in degrees and $rRMSD$ in %, respectively). M and P denote the % magnitude and phase differences.

Normal Walking					
	ρ	$RMSD$	$rRMSD$	M	P
Subtalar Eversion	0.79	9.7 (3.1)	32.6 (10.1)	25.5 (36.2)	18.9 (9.6)
Ankle Plantarflexion	0.95	4.0 (1.3)	13.1 (4.9)	10.3 (16.6)	9.3 (3.6)
Knee Flexion	0.98	4.6 (2.0)	7.4 (3.1)	2.1 (5.5)	4.9 (2.3)
Hip Abduction	0.91	3.9 (1.9)	25.2 (9.1)	-15.9 (28.8)	20.4 (8.0)
Hip External Rotation	0.66	6.5 (2.6)	35.7 (14.1)	7.9 (36.7)	12.6 (5.5)
Hip Flexion	0.99	5.6 (2.2)	12.5 (5.5)	-3.7 (13.0)	8.8 (4.4)

Figure 2: Comfortable walking speed; ankle, knee, and hip joint angle estimates (standard deviation around mean) of the IMC-PGRF (orange shaded area around orange dotted line) and OMC-PGRF models (blue shaded area around blue dashed line) versus OMC-MGRF model (thin black solid lines around thick black solid line).

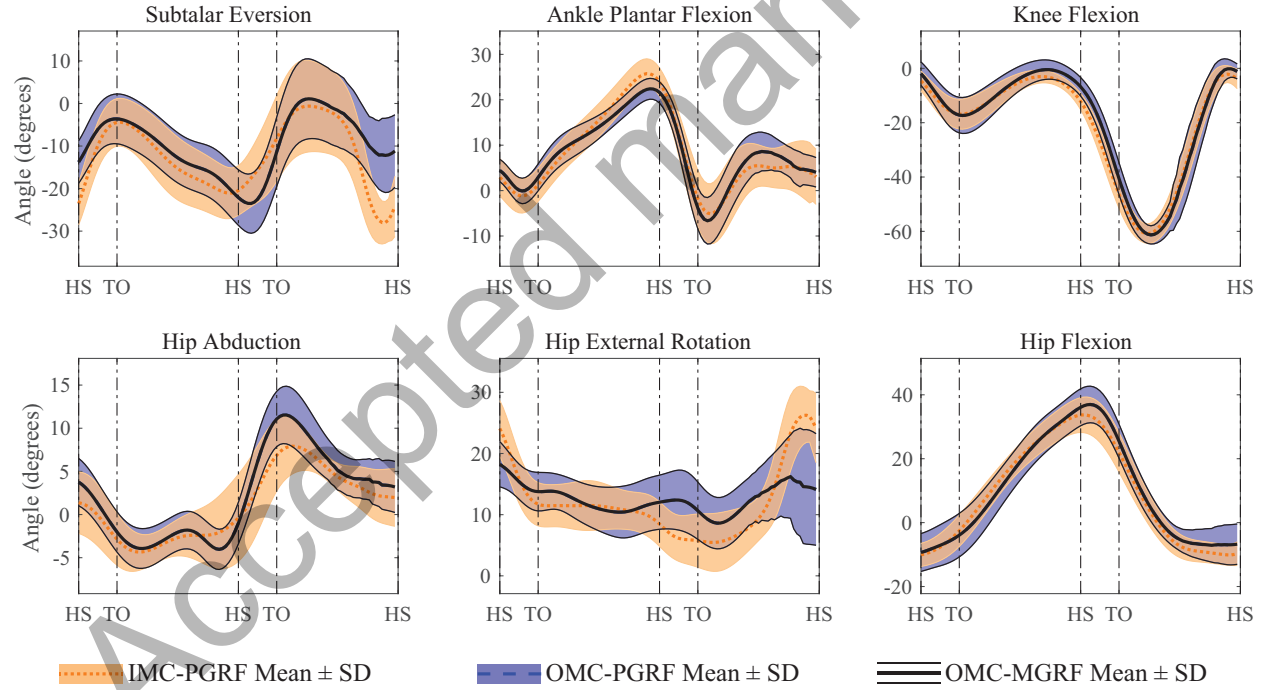


Table 3: Comfortable walking speed; IMC-PGRF-based ground and joint reaction forces (first three quantities) and net moments (second three quantities) versus OMC-MGRF. Pearson correlation coefficient is denoted with ρ . Absolute per body weight (or body weight times height) and relative root-mean-squared-difference are denoted with $RMSD$ (%BW or %BW*BH) and $rRMSD$ (%), respectively. M and P indicate the magnitude and phase differences (%).

	ρ	RMSD	rRMSD	M	P
Ground					
Anteroposterior	0.91	5.5 (1.1)	14.6 (2.4)	-24.8 (6.6)	14.2 (3.0)
Mediolateral	0.80	2.1 (0.5)	18.7 (2.5)	4.8 (17.4)	15.5 (3.0)
Vertical	0.97	8.6 (2.3)	7.1 (1.8)	-1.4 (1.4)	3.1 (0.8)
Frontal	0.66	0.8 (0.5)	34.1 (15.3)	105.5 (334.8)	28.5 (13.8)
Sagittal	0.91	1.5 (0.6)	16.8 (7.0)	12.2 (17.2)	11.6 (4.4)
Transverse	0.83	0.2 (0.1)	22.3 (6.4)	-11.7 (31.7)	17.4 (4.3)
Ankle					
Anteroposterior	0.84	21.9 (10.3)	25.7 (10.1)	48.0 (47.2)	10.9 (2.1)
Mediolateral	0.93	23.9 (8.3)	14.8 (4.9)	12.8 (15.4)	8.0 (2.5)
Proximodistal	0.93	85.6 (27.7)	13.0 (4.4)	8.0 (12.6)	7.2 (2.2)
Eversion	0.75	0.6 (0.2)	31.5 (16.3)	98.7 (234.1)	18.3 (8.6)
Plantar Flexion	0.94	1.5 (0.6)	14.3 (6.0)	8.2 (15.3)	9.6 (3.5)
Axial	0.70	0.5 (0.2)	29.2 (11.6)	38.7 (46.6)	25.4 (12.8)
Knee					
Anteroposterior	0.84	29.8 (9.3)	26.0 (9.8)	49.4 (50.6)	12.3 (4.7)
Mediolateral	0.93	11.4 (3.0)	13.5 (3.8)	8.1 (8.7)	6.4 (2.2)
Proximodistal	0.92	58.4 (29.2)	13.3 (6.9)	5.1 (8.1)	6.7 (3.1)
Abduction	0.83	1.0 (0.4)	17.6 (6.4)	-2.1 (14.7)	10.3 (4.0)
Flexion	0.59	1.8 (0.5)	29.8 (6.8)	16.7 (38.8)	32.9 (8.2)
Axial	0.73	0.3 (0.2)	25.4 (9.9)	2.7 (31.6)	27.8 (13.1)
Hip					
Anteroposterior	0.74	16.7 (7.4)	26.2 (8.8)	5.7 (17.7)	26.6 (8.8)
Mediolateral	0.75	26.1 (13.4)	22.7 (7.6)	7.1 (15.4)	10.3 (4.2)
Proximodistal	0.81	99.0 (25.3)	21.6 (4.4)	21.2 (10.1)	8.5 (2.7)
Abduction	0.84	1.3 (0.7)	18.8 (5.5)	9.5 (17.9)	12.8 (8.2)
Flexion	0.92	2.2 (0.6)	18.9 (3.5)	69.5 (20.9)	14.6 (4.6)
External Rotation	0.47	0.5 (0.2)	30.9 (6.9)	-6.7 (32.6)	25.6 (9.9)

Table 4: Comfortable walking speed; OMC-PGRF-based ground and joint reaction forces (first three quantities) and net moments (second three quantities) versus OMC-MGRF. Pearson correlation coefficient is denoted with ρ . Absolute per body weight (or body weight times height) and relative root-mean-squared-difference are denoted with $RMSD$ (%BW or %BW*BH) and $rRMSD$ (%), respectively. M and P indicate the magnitude and phase differences (%).

	ρ	$RMSD$	$rRMSD$	M	P
Ground					
Anteroposterior	0.96	3.6 (1.0)	8.2 (1.8)	5.8 (8.5)	8.9 (1.8)
Mediolateral	0.77	1.9 (0.4)	19.1 (3.7)	1.6 (10.8)	15.4 (4.1)
Vertical	0.99	5.7 (1.2)	4.8 (1.0)	-1.2 (0.9)	2.1 (0.5)
Frontal	0.66	0.7 (0.2)	30.9 (9.4)	68.9 (139.9)	24.7 (8.2)
Sagittal	0.94	1.1 (0.2)	12.0 (2.6)	15.8 (11.3)	8.4 (2.0)
Transverse	0.82	0.2 (0.1)	19.8 (7.2)	3.8 (21.4)	16.6 (6.4)
Ankle					
Anteroposterior	0.85	18.8 (6.5)	23.2 (6.6)	40.1 (29.7)	10.3 (2.1)
Mediolateral	0.96	15.0 (2.9)	9.8 (1.9)	6.7 (7.5)	5.5 (1.6)
Proximodistal	0.97	57.2 (12.6)	8.8 (2.0)	7.0 (6.7)	4.8 (1.3)
Eversion	0.75	0.5 (0.1)	25.5 (6.8)	45.4 (75.0)	18.0 (8.7)
Plantar Flexion	0.97	0.9 (0.2)	8.9 (2.0)	5.7 (7.3)	6.3 (1.7)
Axial	0.63	0.5 (0.1)	27.3 (6.5)	29.9 (35.3)	26.6 (10.1)
Knee					
Anteroposterior	0.93	11.0 (4.3)	11.2 (2.7)	-6.9 (5.4)	7.2 (1.4)
Mediolateral	0.97	6.5 (1.6)	8.0 (1.8)	-4.2 (3.8)	4.1 (0.7)
Proximodistal	0.96	37.7 (7.8)	8.4 (1.7)	-2.7 (4.0)	4.6 (0.9)
Abduction	0.91	0.7 (0.1)	11.9 (2.3)	-0.3 (8.1)	7.8 (1.7)
Flexion	0.86	0.9 (0.2)	16.7 (4.5)	-1.2 (12.9)	17.2 (5.2)
Axial	0.81	0.2 (0.1)	18.7 (6.2)	-6.5 (17.2)	20.6 (6.9)
Hip					
Anteroposterior	0.89	9.6 (3.0)	15.6 (6.2)	-11.8 (9.3)	16.8 (7.0)
Mediolateral	0.91	14.7 (3.2)	12.6 (2.2)	-2.2 (7.0)	6.4 (1.0)
Proximodistal	0.92	47.5 (13.1)	11.2 (2.2)	-4.9 (4.9)	5.4 (1.0)
Abduction	0.90	0.8 (0.1)	13.3 (2.4)	-3.6 (5.7)	8.9 (2.0)
Flexion	0.86	1.3 (0.3)	16.0 (2.6)	-9.0 (11.8)	17.6 (3.4)
External Rotation	0.67	0.3 (0.1)	22.7 (3.5)	7.0 (15.7)	18.8 (4.4)

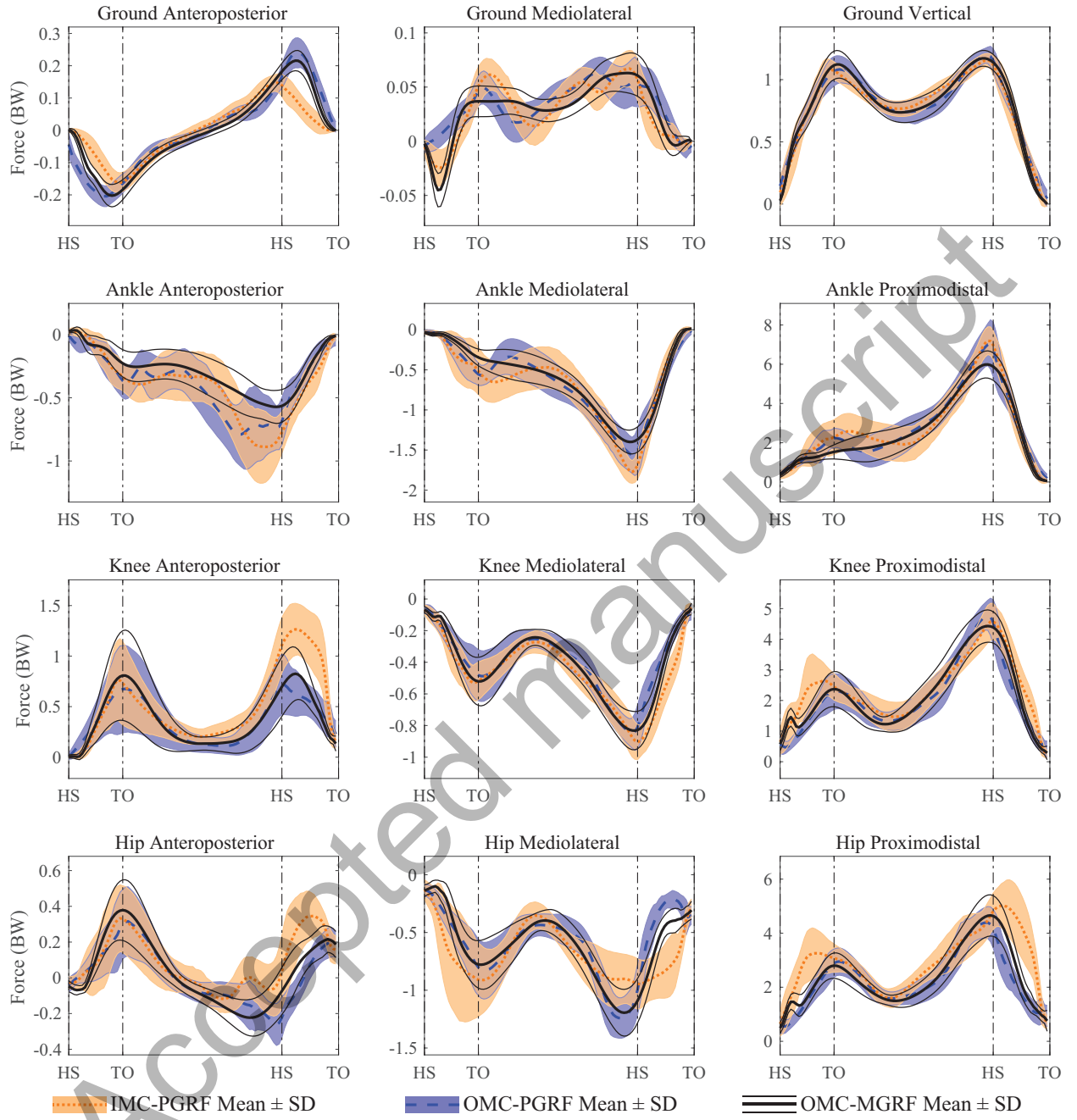


Figure 3: Comfortable walking speed; ground and lower limb joint reaction force estimates (standard deviation around mean) of the IMC-PGRF (orange shaded area around orange dotted line) and OMC-PGRF models (blue shaded area around blue dashed line) versus OMC-MGRF model (thin black solid lines around thick black solid line).

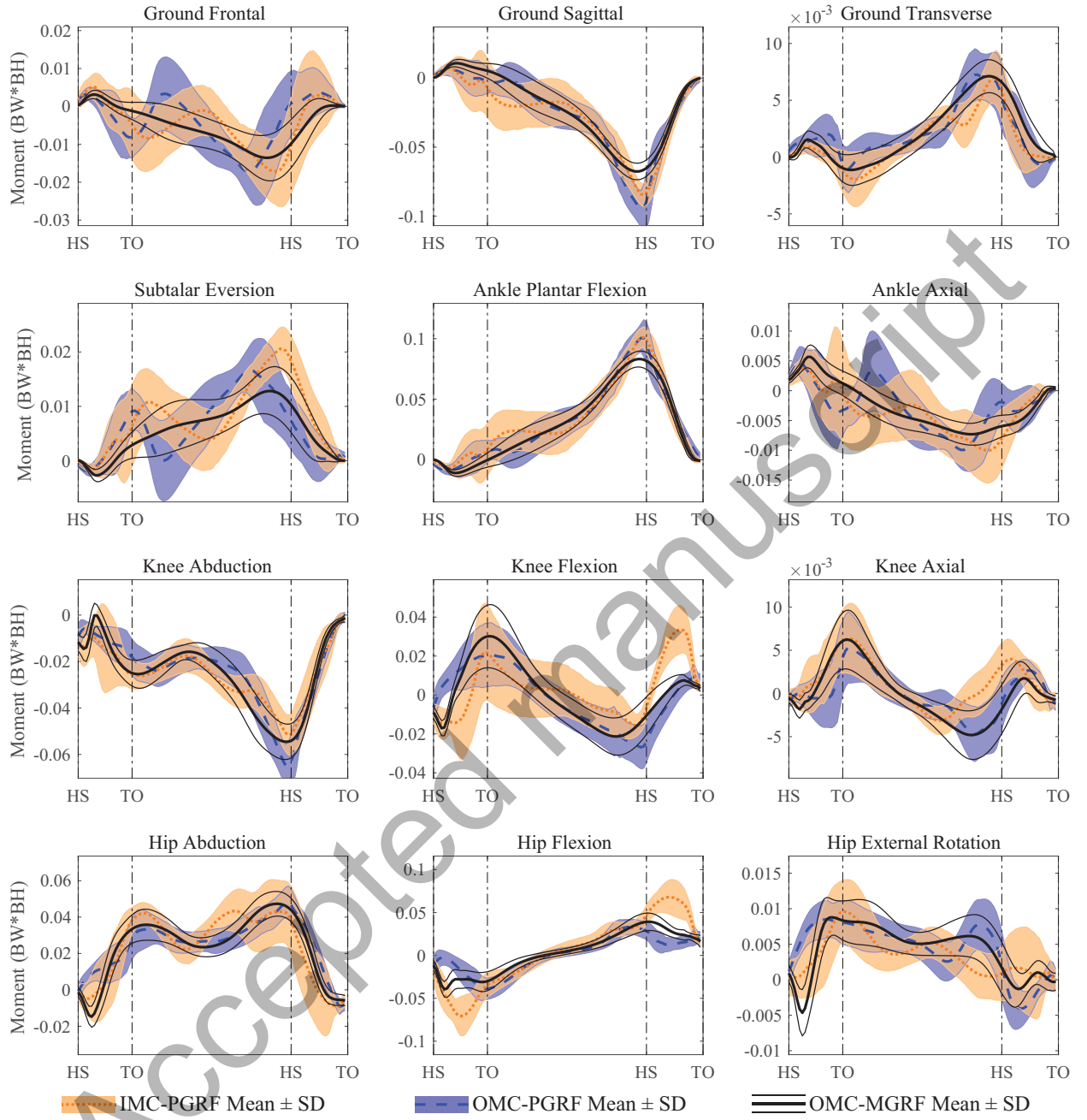


Figure 4: Comfortable walking speed; ground reaction and lower limb net joint moment estimates (standard deviation around mean) of the IMC-PGRF (orange shaded area around orange dotted line) and OMC-PGRF models (blue shaded area around blue dashed line) versus OMC-MGRF model (thin black solid lines around thick black solid line).

2.2. Slow walking speed

Table 5: Slow walking speed; comparison of lower limb joint angles between musculoskeletal model driven by the inertial (IMC-PGRF) and optical motion capture (OMC-PGRF/OMC-MGRF), using Pearson correlation coefficient (ρ), absolute and relative root-mean-squared-differences ($RMSD$ in degrees and $rRMSD$ in %, respectively). M and P denote the % magnitude and phase differences.

Slow Walking					
	ρ	$RMSD$	$rRMSD$	M	P
	Corr	RMSE	rRMSE	M	P
Subtalar Eversion	0.81	10.1 (3.5)	32.9 (9.6)	29.5 (36.3)	17.6 (10.1)
Ankle Plantarflexion	0.96	3.9 (1.2)	13.7 (4.0)	5.1 (14.0)	9.5 (3.4)
Knee Flexion	0.99	4.1 (2.4)	7.0 (4.3)	-0.3 (7.5)	4.7 (3.6)
Hip Abduction	0.91	4.1 (2.1)	27.6 (12.4)	-3.3 (42.8)	23.2 (10.9)
Hip External Rotation	0.76	6.7 (3.1)	39.5 (17.9)	12.9 (46.9)	13.0 (6.7)
Hip Flexion	0.99	5.2 (1.9)	13.3 (5.7)	-3.8 (16.4)	8.6 (4.2)

Figure 5: Slow walking speed; ankle, knee, and hip joint angle estimates (standard deviation around mean) of the IMC-PGRF (orange shaded area around orange dotted line) and OMC-PGRF models (blue shaded area around blue dashed line) versus OMC-MGRF model (thin black solid lines around thick black solid line).

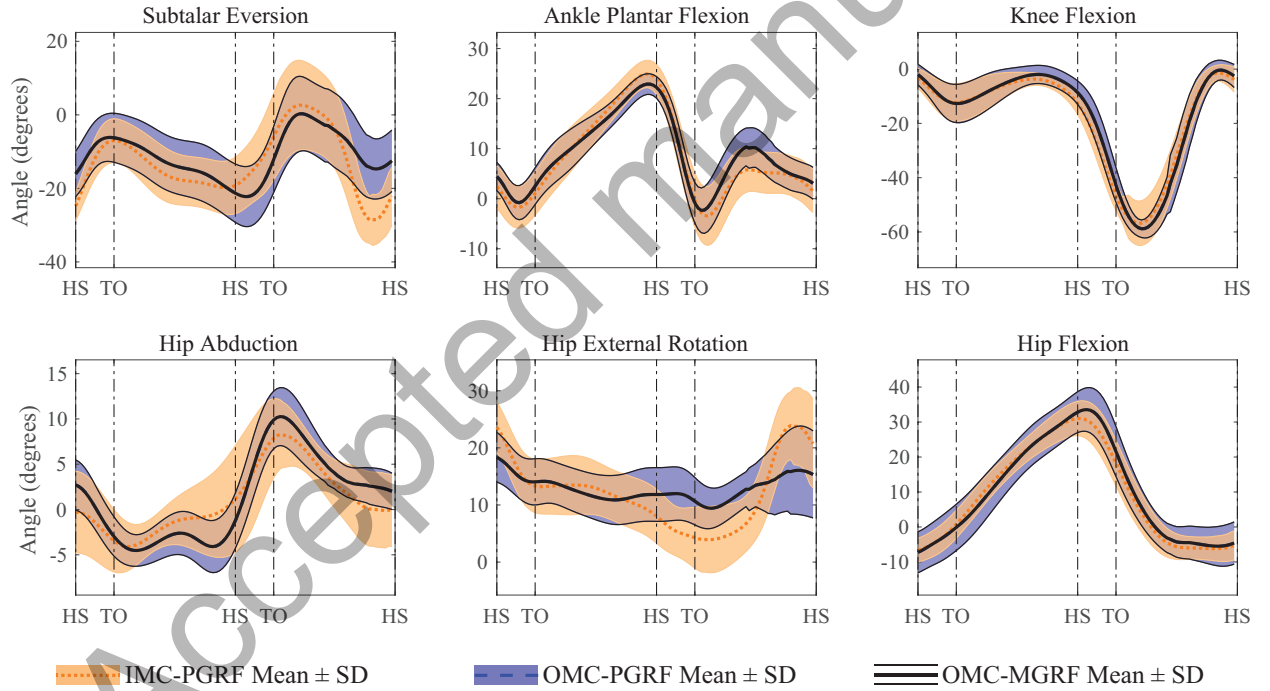


Table 6: Slow walking speed; IMC-PGRF-based ground and joint reaction forces (first three quantities) and net moments (second three quantities) versus OMC-MGRF. Pearson correlation coefficient is denoted with ρ . Absolute per body weight (or body weight times height) and relative root-mean-squared-difference are denoted with $RMSD$ (%BW or %BW*BH) and $rRMSD$ (%), respectively. M and P indicate the magnitude and phase differences (%).

	ρ	RMSD	rRMSD	M	P
Ground					
Anteroposterior	0.88	4.7 (0.8)	16.3 (2.3)	-26.3 (8.6)	15.8 (3.4)
Mediolateral	0.84	1.7 (0.5)	17.6 (3.6)	13.2 (23.1)	13.3 (3.5)
Vertical	0.97	8.1 (2.3)	7.4 (2.1)	-1.5 (1.2)	3.0 (0.9)
Frontal	0.64	1.0 (0.8)	45.7 (32.5)	177.8 (340.9)	32.6 (21.9)
Sagittal	0.90	1.5 (0.7)	18.7 (8.2)	10.2 (20.2)	12.2 (4.9)
Transverse	0.81	0.2 (0.1)	23.3 (5.8)	-0.7 (56.1)	17.5 (4.7)
Ankle					
Anteroposterior	0.85	22.8 (12.2)	29.0 (12.1)	56.5 (52.1)	10.7 (2.5)
Mediolateral	0.93	24.2 (11.3)	16.0 (6.7)	12.9 (21.3)	7.7 (2.9)
Proximodistal	0.93	87.4 (38.0)	14.3 (5.6)	8.2 (18.1)	7.1 (2.3)
Eversion	0.78	0.6 (0.3)	37.6 (27.2)	140.7 (259.7)	18.7 (13.5)
Plantar Flexion	0.93	1.6 (0.8)	16.8 (8.5)	9.6 (24.0)	10.1 (4.1)
Axial	0.65	0.5 (0.2)	33.7 (14.9)	47.8 (61.5)	27.9 (15.2)
Knee					
Anteroposterior	0.84	23.6 (6.8)	25.9 (11.3)	50.0 (65.3)	11.5 (3.0)
Mediolateral	0.89	10.5 (3.1)	14.7 (4.2)	3.8 (7.4)	7.3 (2.1)
Proximodistal	0.87	65.0 (29.7)	16.8 (7.3)	5.2 (11.7)	8.1 (3.1)
Abduction	0.74	1.2 (0.5)	23.2 (7.5)	-5.8 (20.4)	12.0 (4.5)
Flexion	0.46	1.8 (0.5)	34.5 (7.2)	35.3 (59.5)	36.9 (10.3)
Axial	0.60	0.3 (0.1)	29.8 (10.7)	8.2 (32.3)	33.0 (14.6)
Hip					
Anteroposterior	0.55	17.3 (7.2)	32.5 (10.3)	11.0 (30.6)	34.7 (12.2)
Mediolateral	0.66	23.8 (11.1)	25.1 (7.4)	5.8 (15.0)	11.1 (4.4)
Proximodistal	0.71	88.4 (23.7)	23.1 (3.8)	17.8 (8.4)	9.3 (2.4)
Abduction	0.83	1.4 (0.7)	21.0 (6.9)	-1.1 (13.4)	14.0 (8.3)
Flexion	0.92	2.0 (0.4)	22.8 (3.5)	93.3 (23.2)	15.5 (4.1)
External Rotation	0.57	0.4 (0.2)	32.4 (7.0)	-0.2 (40.5)	24.8 (10.4)

Table 7: Slow walking speed; OMC-PGRF-based ground and joint reaction forces (first three quantities) and net moments (second three quantities) versus OMC-MGRF. Pearson correlation coefficient is denoted with ρ . Absolute per body weight (or body weight times height) and relative root-mean-squared-difference are denoted with $RMSD$ (%BW or %BW*BH) and $rRMSD$ (%), respectively. M and P indicate the magnitude and phase differences (%).

	ρ	$RMSD$	$rRMSD$	M	P
Ground					
Anteroposterior	0.97	3.2 (1.2)	8.8 (2.6)	16.5 (13.0)	8.5 (1.7)
Mediolateral	0.82	1.5 (0.3)	17.2 (2.8)	4.4 (10.9)	13.8 (4.3)
Vertical	0.99	5.1 (1.6)	4.7 (1.5)	-1.4 (1.4)	1.8 (0.6)
Frontal	0.70	0.6 (0.2)	29.7 (10.2)	83.9 (124.3)	22.3 (9.5)
Sagittal	0.94	1.1 (0.4)	13.4 (5.0)	5.0 (12.4)	9.7 (4.2)
Transverse	0.80	0.2 (0.1)	21.2 (6.9)	16.2 (24.5)	18.1 (7.9)
Ankle					
Anteroposterior	0.83	16.8 (6.8)	22.7 (6.2)	32.4 (31.0)	11.2 (2.8)
Mediolateral	0.96	14.4 (3.8)	10.6 (3.1)	1.9 (10.0)	5.6 (2.4)
Proximodistal	0.97	55.3 (16.7)	9.8 (3.5)	1.2 (8.9)	5.2 (2.3)
Eversion	0.79	0.4 (0.1)	24.7 (8.3)	43.2 (59.0)	18.0 (13.3)
Plantar Flexion	0.96	0.9 (0.4)	10.6 (4.4)	-0.9 (9.2)	7.2 (3.2)
Axial	0.68	0.4 (0.1)	27.3 (7.3)	37.2 (42.0)	25.6 (11.9)
Knee					
Anteroposterior	0.92	9.9 (3.5)	14.8 (5.7)	-11.4 (11.5)	7.6 (2.7)
Mediolateral	0.96	7.0 (2.4)	9.9 (3.5)	-7.3 (6.1)	4.6 (1.3)
Proximodistal	0.95	39.1 (14.7)	10.1 (3.6)	-6.8 (5.6)	5.0 (1.6)
Abduction	0.90	0.7 (0.1)	14.0 (2.9)	-5.3 (11.3)	7.7 (1.6)
Flexion	0.84	0.8 (0.2)	18.7 (5.4)	-2.8 (18.0)	18.2 (5.8)
Axial	0.73	0.2 (0.1)	21.7 (7.0)	2.7 (16.2)	24.7 (9.2)
Hip					
Anteroposterior	0.87	8.3 (2.7)	17.0 (7.4)	-10.0 (9.0)	18.4 (9.3)
Mediolateral	0.90	12.9 (4.3)	13.7 (3.9)	-2.3 (5.7)	6.5 (2.0)
Proximodistal	0.91	44.3 (13.9)	12.4 (3.0)	-6.0 (5.9)	5.5 (1.3)
Abduction	0.93	0.7 (0.1)	12.4 (2.7)	-2.4 (6.2)	7.1 (1.7)
Flexion	0.81	1.1 (0.3)	19.2 (2.4)	-12.4 (11.7)	20.7 (3.3)
External Rotation	0.71	0.3 (0.1)	22.4 (4.1)	12.5 (16.0)	16.9 (4.2)

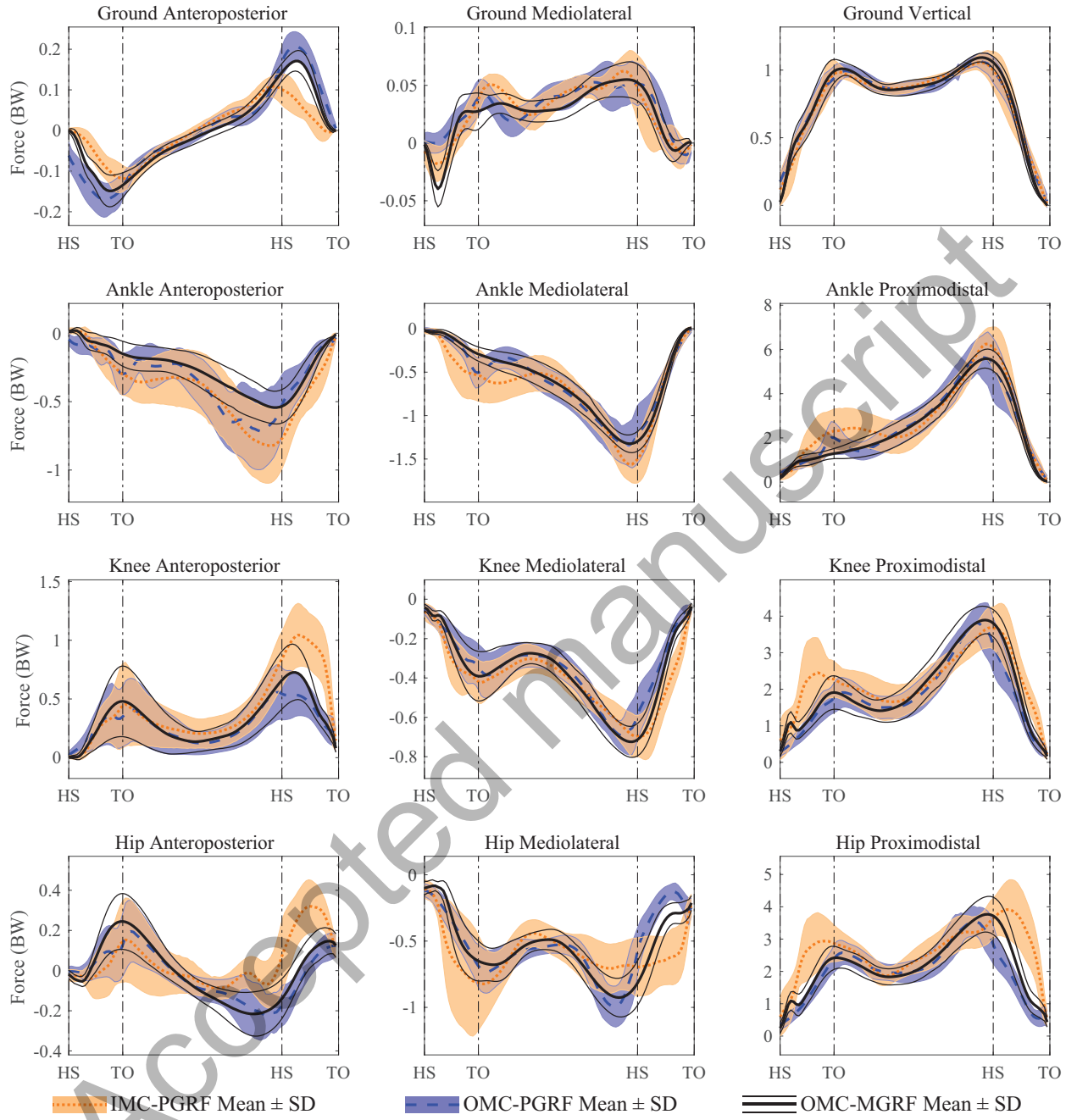


Figure 6: Slow walking speed; ground and lower limb joint reaction force estimates (standard deviation around mean) of the IMC-PGRF (orange shaded area around orange dotted line) and OMC-PGRF models (blue shaded area around blue dashed line) versus OMC-MGRF model (thin black solid lines around thick black solid line).

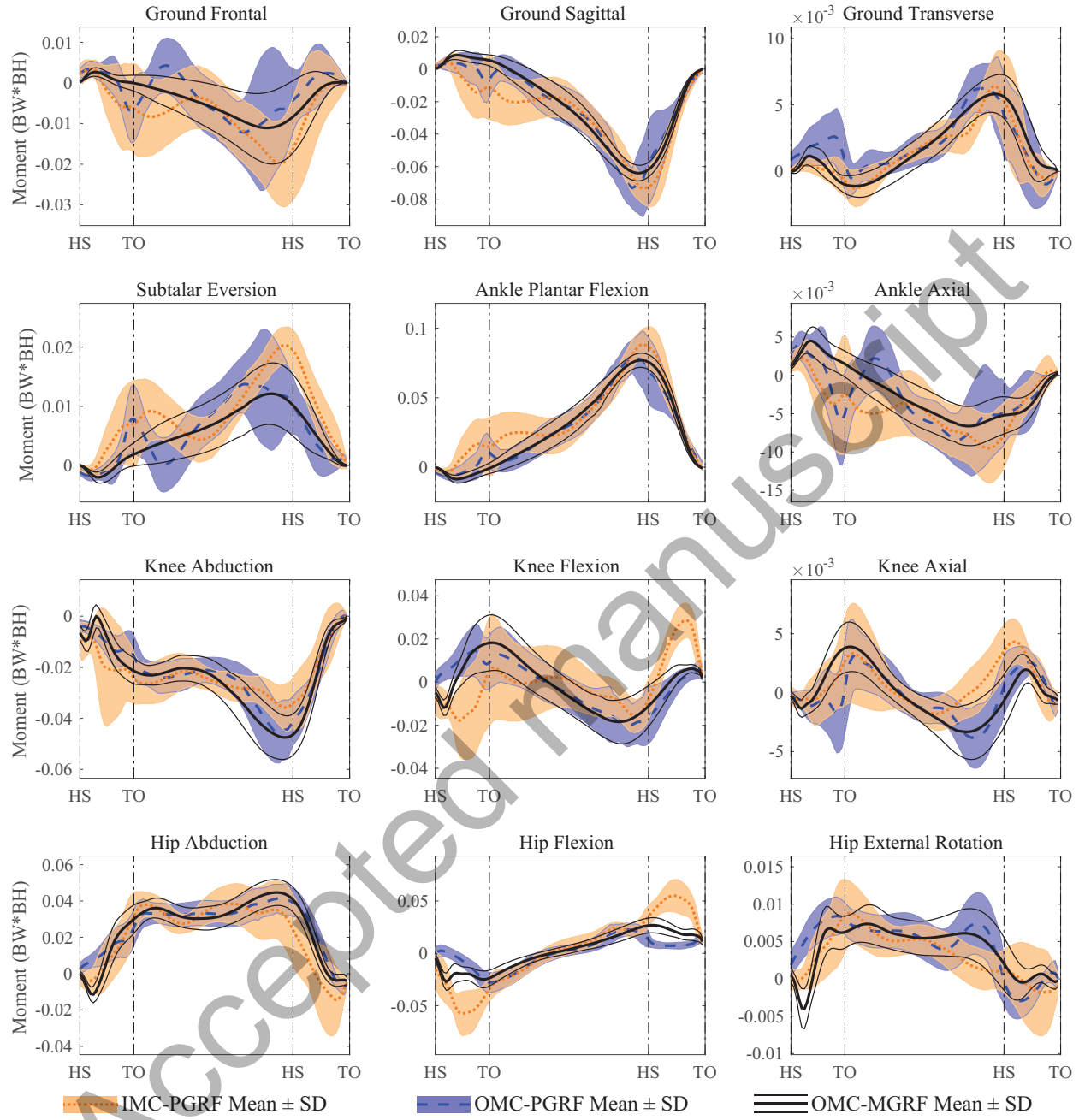


Figure 7: Slow walking speed; ground reaction and lower limb net joint moment estimates (standard deviation around mean) of the IMC-PGRF (orange shaded area around orange dotted line) and OMC-PGRF models (blue shaded area around blue dashed line) versus OMC-MGRF model (thin black solid lines around thick black solid line).

2.3. Fast walking speed

Table 8: Fast walking speed; comparison of lower limb joint angles between musculoskeletal model driven by the inertial (IMC-PGRF) and optical motion capture (OMC-PGRF/OMC-MGRF), using Pearson correlation coefficient (ρ), absolute and relative root-mean-squared-differences ($RMSD$ in degrees and $rRMSD$ in %, respectively). M and P denote the % magnitude and phase differences.

Fast Walking					
	ρ	$RMSD$	$rRMSD$	M	P
Subtalar Eversion	0.83	9.3 (2.8)	32.2 (11.4)	16.1 (29.9)	21.6 (10.9)
Ankle Plantarflexion	0.95	4.6 (1.3)	15.4 (5.1)	10.4 (18.3)	10.8 (4.7)
Knee Flexion	0.98	4.6 (1.6)	7.3 (2.6)	-0.0 (5.0)	4.6 (1.9)
Hip Abduction	0.9	4.2 (2.0)	25.0 (10.3)	-17.6 (29.6)	20.0 (8.4)
Hip External Rotation	0.62	6.2 (2.6)	35.3 (12.8)	-5.4 (29.1)	12.0 (6.4)
Hip Flexion	0.99	6.3 (1.9)	12.5 (4.4)	-4.6 (12.0)	9.1 (3.8)

Figure 8: Fast walking speed; ankle, knee, and hip joint angle estimates (standard deviation around mean) of the IMC-PGRF (orange shaded area around orange dotted line) and OMC-PGRF models (blue shaded area around blue dashed line) versus OMC-MGRF model (thin black solid lines around thick black solid line).

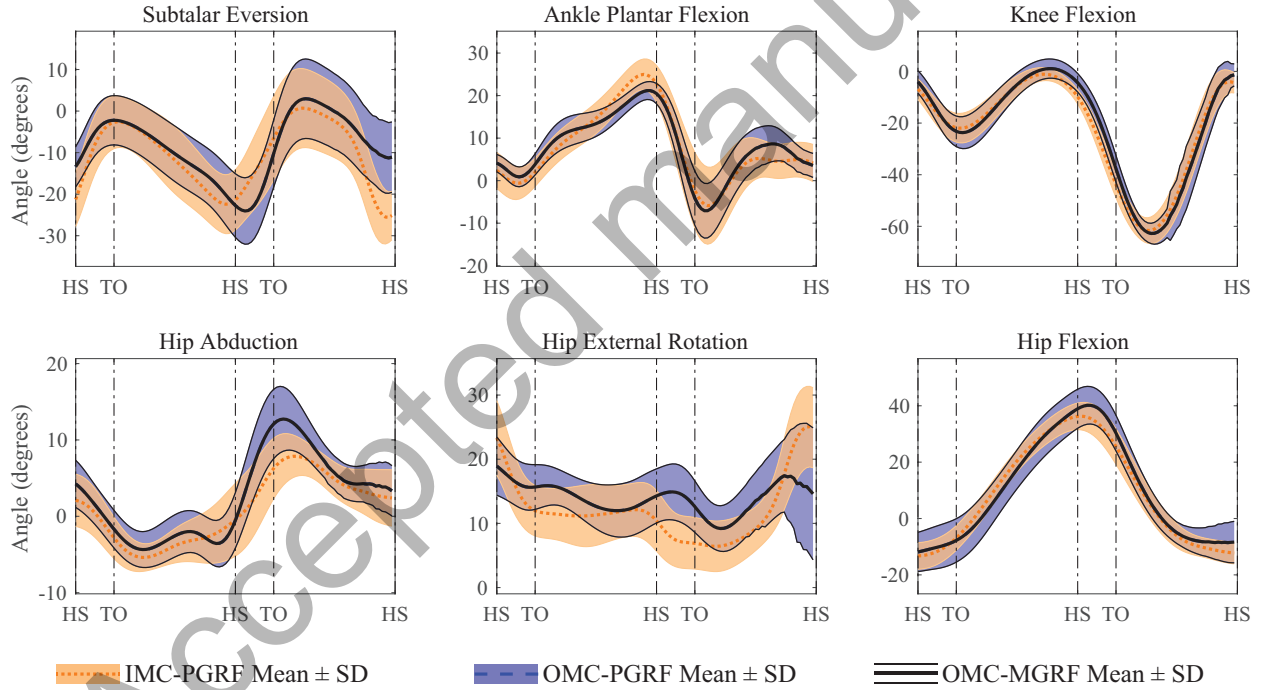


Table 9: Fast walking speed; IMC-PGRF-based ground and joint reaction forces (first three quantities) and net moments (second three quantities) versus OMC-MGRF. Pearson correlation coefficient is denoted with ρ . Absolute per body weight (or body weight times height) and relative root-mean-squared-difference are denoted with $RMSD$ (%BW or %BW*BH) and $rRMSD$ (%), respectively. M and P indicate the magnitude and phase differences (%).

	ρ	RMSD	rRMSD	M	P
Ground					
Anteroposterior	0.92	6.5 (1.2)	14.1 (2.0)	-25.2 (6.6)	13.0 (2.7)
Mediolateral	0.75	2.5 (0.7)	19.3 (3.4)	3.9 (15.2)	17.5 (3.8)
Vertical	0.95	11.5 (3.2)	8.8 (2.2)	-1.7 (1.8)	4.1 (1.1)
Frontal	0.61	0.9 (0.5)	34.1 (15.5)	91.7 (269.9)	30.9 (15.0)
Sagittal	0.90	1.7 (0.4)	17.1 (4.2)	21.6 (15.2)	12.7 (4.1)
Transverse	0.81	0.2 (0.1)	24.4 (9.3)	-13.1 (33.0)	18.4 (6.8)
Ankle					
Anteroposterior	0.84	22.0 (8.0)	23.4 (6.9)	41.8 (34.5)	10.7 (1.5)
Mediolateral	0.94	25.0 (6.2)	14.9 (3.7)	17.7 (13.1)	8.0 (2.9)
Proximodistal	0.93	93.3 (23.8)	13.6 (3.2)	13.8 (9.3)	7.5 (2.5)
Eversion	0.75	0.7 (0.2)	30.7 (13.7)	81.9 (137.1)	19.8 (9.8)
Plantar Flexion	0.93	1.6 (0.4)	14.1 (4.2)	14.8 (12.5)	10.1 (3.3)
Axial	0.65	0.6 (0.1)	28.3 (8.4)	54.9 (33.2)	28.6 (12.1)
Knee					
Anteroposterior	0.75	39.4 (8.2)	25.3 (7.4)	29.3 (38.3)	15.7 (4.6)
Mediolateral	0.90	14.5 (3.0)	14.3 (3.3)	8.0 (8.9)	7.3 (1.5)
Proximodistal	0.92	66.8 (19.0)	12.8 (4.0)	5.0 (7.0)	6.7 (1.8)
Abduction	0.86	1.1 (0.2)	15.5 (3.3)	0.1 (10.9)	9.8 (2.1)
Flexion	0.67	2.0 (0.4)	24.6 (5.3)	-0.2 (18.7)	28.2 (8.3)
Axial	0.83	0.3 (0.1)	20.6 (8.1)	-4.9 (25.8)	22.2 (11.5)
Hip					
Anteroposterior	0.80	19.0 (8.3)	22.5 (6.7)	3.3 (23.4)	20.7 (5.9)
Mediolateral	0.77	31.8 (11.6)	21.1 (6.8)	10.5 (13.0)	10.6 (3.7)
Proximodistal	0.82	123.9 (32.5)	20.3 (4.9)	21.7 (11.2)	9.2 (2.4)
Abduction	0.80	1.5 (0.6)	19.5 (4.5)	10.7 (16.6)	14.4 (6.9)
Flexion	0.91	2.6 (0.6)	16.4 (3.1)	55.2 (20.0)	14.5 (3.8)
External Rotation	0.44	0.5 (0.2)	31.7 (5.6)	-4.5 (36.2)	26.6 (9.9)

Table 10: Fast walking speed; OMC-PGRF-based ground and joint reaction forces (first three quantities) and net moments (second three quantities) versus OMC-MGRF. Pearson correlation coefficient is denoted with ρ . Absolute per body weight (or body weight times height) and relative root-mean-squared-difference are denoted with *RMSD* (%BW or %BW*BH) and *rRMSD* (%), respectively. *M* and *P* indicate the magnitude and phase differences (%).

	ρ	RMSD	rRMSD	M	P
Ground					
Anteroposterior	0.96	4.2 (0.8)	7.9 (1.5)	0.1 (7.4)	9.0 (1.7)
Mediolateral	0.76	2.2 (0.5)	19.4 (5.3)	1.2 (10.6)	16.5 (6.0)
Vertical	0.98	7.2 (2.3)	5.4 (1.6)	-1.0 (0.9)	2.6 (0.8)
Frontal	0.59	0.8 (0.2)	30.1 (8.1)	59.1 (92.8)	26.9 (9.3)
Sagittal	0.94	1.5 (0.3)	14.3 (2.9)	28.3 (13.3)	9.7 (2.8)
Transverse	0.80	0.2 (0.1)	21.0 (8.5)	1.1 (19.8)	17.9 (8.3)
Ankle					
Anteroposterior	0.83	21.3 (7.0)	22.9 (5.2)	39.4 (23.6)	11.0 (1.9)
Mediolateral	0.95	19.4 (4.2)	11.9 (2.3)	12.5 (8.6)	6.6 (2.2)
Proximodistal	0.96	76.4 (15.8)	11.0 (2.0)	13.7 (6.9)	5.7 (1.7)
Eversion	0.72	0.6 (0.1)	26.2 (5.6)	47.5 (55.2)	20.3 (7.5)
Plantar Flexion	0.96	1.3 (0.3)	10.9 (2.6)	13.8 (8.0)	7.7 (2.7)
Axial	0.60	0.5 (0.1)	27.0 (8.2)	33.3 (32.7)	30.6 (12.1)
Knee					
Anteroposterior	0.94	15.2 (4.1)	10.8 (2.3)	-3.0 (5.8)	7.4 (1.6)
Mediolateral	0.96	8.2 (1.6)	8.5 (1.4)	-0.6 (4.7)	4.5 (0.8)
Proximodistal	0.95	49.6 (9.0)	9.4 (1.6)	1.7 (4.7)	5.3 (0.9)
Abduction	0.92	0.9 (0.2)	11.8 (1.8)	6.1 (9.0)	7.6 (1.5)
Flexion	0.90	1.2 (0.3)	14.6 (3.4)	-1.1 (11.2)	15.2 (4.0)
Axial	0.89	0.2 (0.1)	14.8 (4.7)	-6.5 (18.5)	16.1 (4.9)
Hip					
Anteroposterior	0.91	11.9 (4.0)	15.4 (6.4)	-9.1 (13.3)	14.4 (5.4)
Mediolateral	0.94	16.6 (3.5)	11.7 (2.4)	-1.2 (7.9)	5.8 (1.2)
Proximodistal	0.93	59.5 (17.0)	10.8 (2.5)	-2.6 (7.2)	5.5 (1.3)
Abduction	0.88	1.0 (0.2)	14.3 (2.5)	-3.5 (7.2)	10.4 (2.4)
Flexion	0.89	1.6 (0.3)	13.8 (2.9)	-6.1 (13.0)	15.3 (3.8)
External Rotation	0.67	0.4 (0.1)	22.2 (3.5)	-0.9 (12.6)	20.7 (5.3)

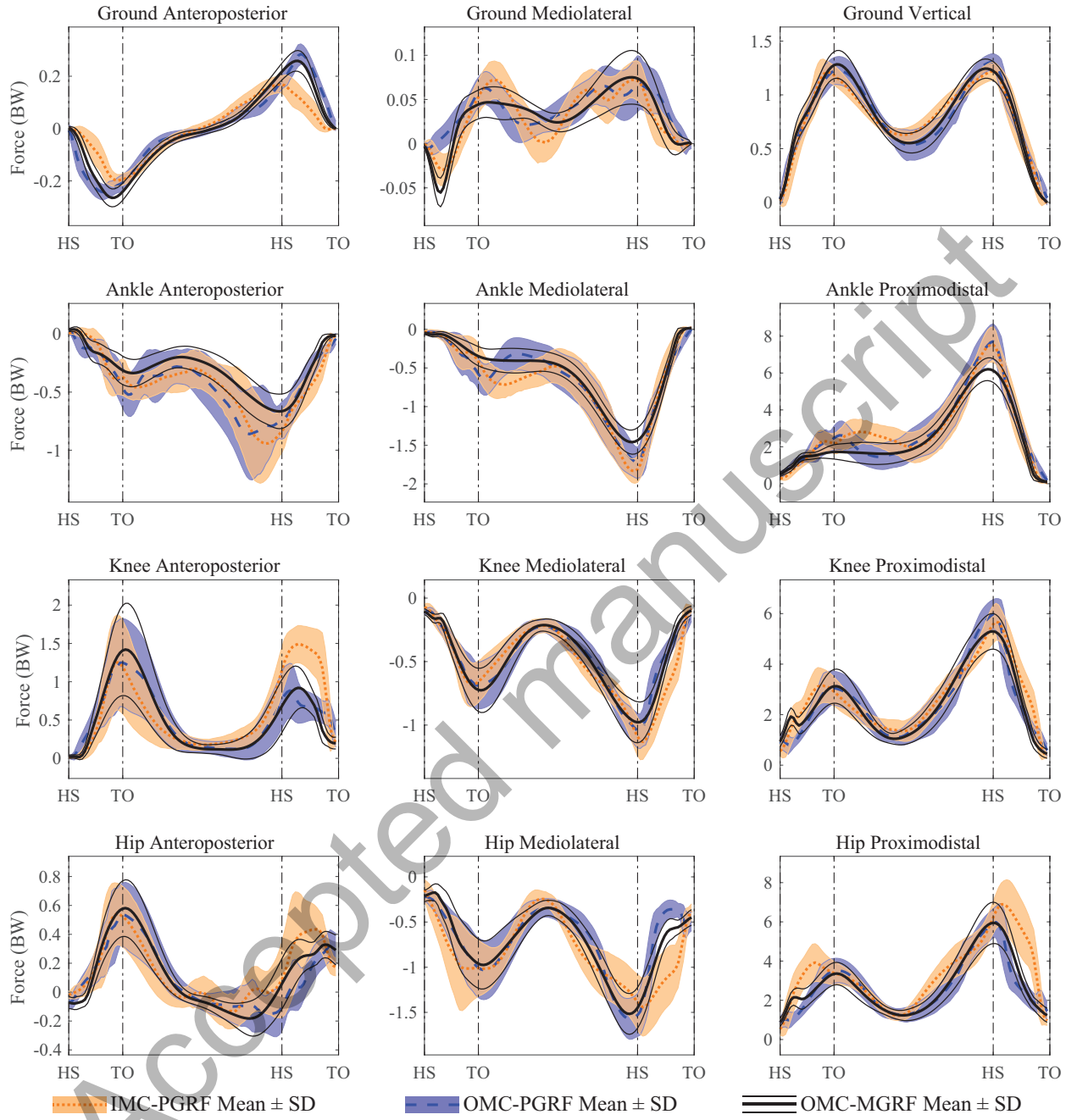


Figure 9: Fast walking speed; ground and lower limb joint reaction force estimates (standard deviation around mean) of the IMC-PGRF (orange shaded area around orange dotted line) and OMC-PGRF models (blue shaded area around blue dashed line) versus OMC-MGRF model (thin black solid lines around thick black solid line).

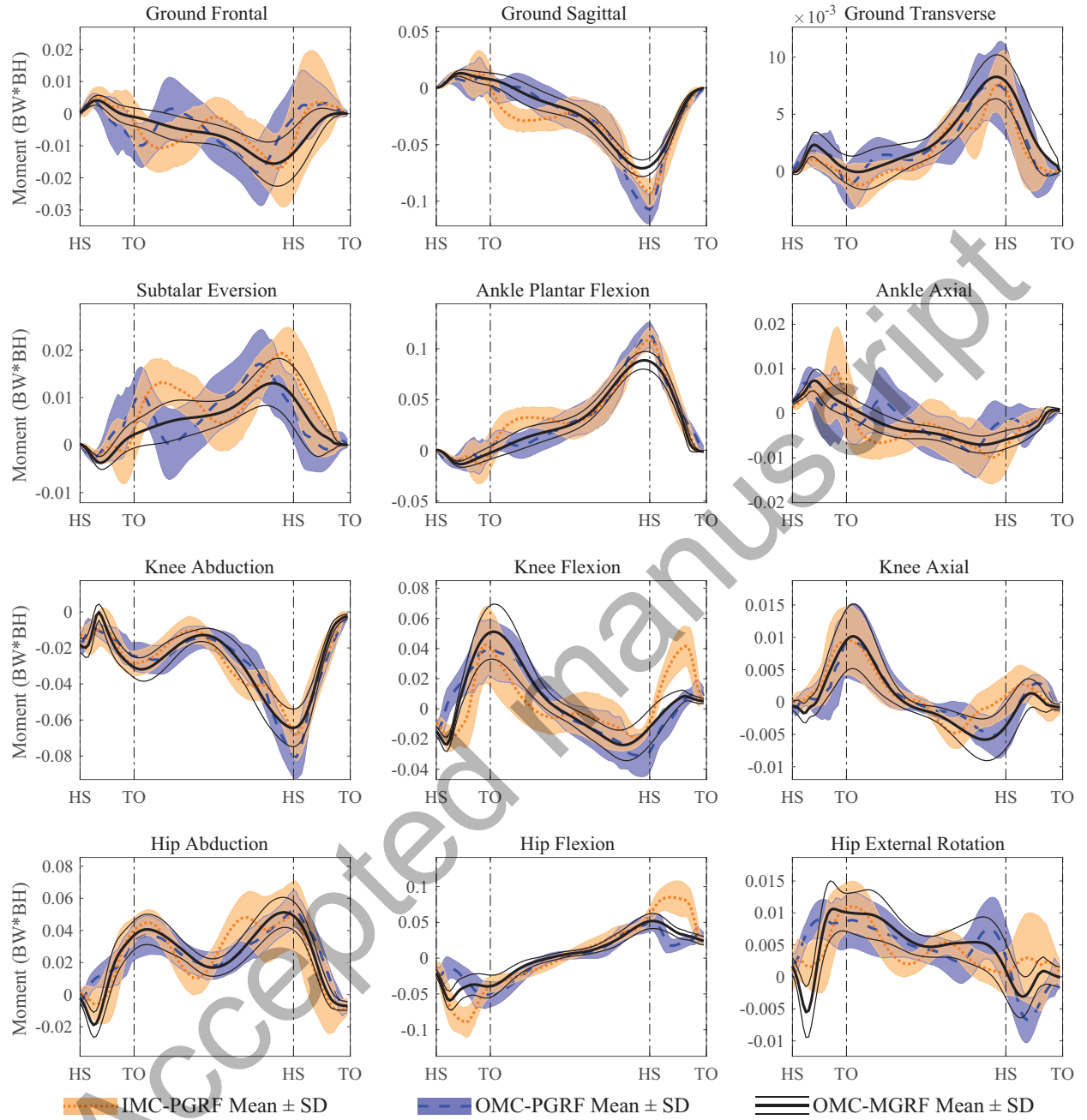


Figure 10: Fast walking speed; ground reaction and lower limb net joint moment estimates (standard deviation around mean) of the IMC-PGRF (orange shaded area around orange dotted line) and OMC-PGRF models (blue shaded area around blue dashed line) versus OMC-MGRF model (thin black solid lines around thick black solid line).